Morphology of the Wide Bay Inlet Ebb-tidal delta, 1987-2009, as observed through Landsat 5 and Landsat 7 imagery.

A multidecadal analysis of ebb delta morphological variation using optical satellite imagery derived nearshore topographies.

Annette Burke

A thesis submitted as a requirement to fulfil the degree of Masters of Research

Department of Environment and Geography

Faculty of Science

Macquarie University

October 2014

Statement of Candidate

I certify that the work in this thesis entitled "Morphology of the Wide Bay Ebb-tidal delta, 1987-2009, as observed through Landsat 5 imagery" has not previously been submitted for a degree nor has it been submitted as part of requirements for a degree to any other university or institution other then Macquarie University.

I also certify that the thesis is an original piece of research and it has been written by me. Any help and assistance that I have received in my research work and the preparation of the thesis itself have been appropriately acknowledged.

In addition, I certify that all information sources and literature used are indicated in the thesis.

Annette Burke (84045442)

10 October 2014

Acknowledgements

The completion of this research would not have been possible without the encouragement, support and advice provided by my supervisors, Associate Professor Ian Goodwin and Dr Michael Chang. To the other members of the Department of Environment and Geography who provided support to Master of Research candidates, a sincere thank you. Finally to my dearest 'inner sanctum'- you know who you are- I would achieve nothing without you all.

Contents

Table of Figures

Abstract

The morphology of ebb-tidal deltas, found on the seaward side of tidal inlets, is shaped by the relative strength of tide and wave generated currents, frequency and intensity of storms and overall sediment supply within the coastal compartment. In micro-tidal environments, ebb-tidal deltas are predominantly below the low water mark, and so detailed observational studies of morphological evolution have been hampered by the difficulties in obtaining regular time series benthic terrain data in the near shore zone. The aim of this study is to investigate the evolution of the ebb-tidal delta at the Wide Bay Inlet from 1987 to 2009. Benthic surfaces for each year were derived from relative depth values generated by implementing a ratio transform algorithm developed by Stumpf et al. (2003), based on the differential attenuation of light at blue and green wavelengths as a function of depth. Changes between the resultant relative depth surfaces evidence movement of the morphological elements of the ebb-tidal delta complex as well as patterns of sediment movement onto the shoreline and associated patterns of shoreline progradation and erosion. Spatial variability of the main ebb-tidal elements and the periodicity of these variations are documented and compared to conceptual models of ebb-tidal delta behaviour.

1 Beneath the surface

1.1 Research Aims

Understanding morphological evolution in shallow water nearshore zones has been hindered by difficulty in making regular observations of the benthos. This study investigates the potential to generate a multidecadal record of changes in the ebb-tidal delta at Wide Bay, SE Queensland (25.828655°S, 153.067349°E) using bathymetric data generated from images in the Landsat multispectral image archive, and to analyse this record for evidence of morphological variation related to natural forcing. The size of the ebb-tidal delta at Wide Bay (approximately 60km^2) makes it suitable for observation from satellite sensors, and because the inlet is not engineered, morphological change can be directly related to natural forcing. Landsat multispectral imagery was chosen over other sensor data because of the following factors: the length of the archive – almost four decades of data collected at 16 day intervals; it is freely available; the spatial resolution of the data (30metre pixel size) is suited to feature analysis; Landsat sensor radiometric calibration in the visible and near infra-red spectrum is suitable for shallow water depth analysis. Bathymetric surfaces were generated using an empirical algorithm developed by Stumpf et al. (2003) based on the differential attenuation of reflectance values for light in blue and green bandwidths. The algorithm can be implemented without the need for in-situ coefficient measurements as is the case with analytic methods and has been shown to produce depth data to an accuracy suitable to analysis of morphological variability (Pe'eri et al., 2014, Collin and Hench, 2012).

1.2 Coastal Geomorpholgy

Coastal geomorphology as a discipline investigates the interaction of marine, atmospheric, geological and anthropogenic systems (Sherman, 2013). The coastal environment is inherently dynamic, with morphologies being shaped by oceanic and atmospheric processes operating upon geological and anthropogenic controls experienced at particular sites (Sherman, 2013). Coastal morphology results from the interaction of geomorphology, climate, hydrodynamics and sediment supply (Perillo and Piccolo, 2011). Geomorphological characteristics - shelf margin, stability and lithology –set the boundary conditions upon which climatically generated forcing agents- wind, waves, ocean currents- interact with system

sediment supply and sediment transport into, out of and along coastal units. The interaction of these elements can be understood to have differing but interconnected morphological effects depending on the spatial and temporal scales of investigation. It has been observed that understandings of coastal morphological variability at synoptic to inter-annual scales and conversely geologic timeframes is well developed. However at decadal to millennial timescales there is much less certainty (Woodroffe and Murray-Wallace, 2012). Morphological variability at decadal to millennial time scales is evident in shoreline movement and beach rotations and large scale sedimentary cycles encompassing major storm erosion and recovery, driven by oscillations in wave climate generated by prevalent atmospheric forcing mechanisms (Short and Jackson, 2013). This decadal to millennial variability, classified as Large Scale Coastal Behaviour (LSCB), is particularly pertinent for coastal planning as investigations into the extent, patterns and drivers of naturally occurring coastal variability at this scale can provide insights into the impact of climate change, particularly with regards to sea level increase and wave climate variation (FitzGerald et al., 2008, Short and Jackson, 2013).

The dynamism of the land-ocean interface is a product of the reworking of sediment between the backshore, upper shoreface and the lower shoreface, driven by environmental forcing, and sediment supply into and out of coastal compartments due to longshore transport (Harley et al., 2011, Cowell et al., 2003a). While variability of the subaerial coast has a long history of documentation and investigation, the variability of the subaqueous or nearshore section of coastal compartments is less understood because of the difficulty in conducting and documenting surveys of the nearshore (Ruggiero et al., 2005).

Both traditional and more recent technologies have limited investigation of nearshore morphological change. Vessel based lead-line, sonar and acoustic sounding methods are limited to navigable depths while air-borne LiDAR sensors have, until recently been, ill-suited to very shallow waters on coastal fringes (Lyzenga et al., 2006, Gao, 2009, Leon et al., 2013). Both technologies are expensive and are implemented on limited spatial extents, due to platform limitations and cost considerations (Lyzenga et al., 2006, Hu, 2008). In order to investigate the morphology of the nearshore at larger spatial scales or in areas that are unlikely or unable to be surveyed by sonar or LiDAR technologies, multispectral and hyperspectral satellite imagery has been interrogated. Bathymetries are retrieved using

principles of light transmission in water where the amount of energy reflected from a water column is understood to be related to wavelength and is a function of water depth (Gao, 2009, Bierwirth et al., 1993). A variety of algorithms have been developed, both physically based and empirical, that require differing levels of in situ co-efficient tuning (Lyzenga, 1978, Lyzenga et al., 2006, Stumpf et al., 2003, Philpot, 1989, Su et al., 2014). There has been extensive research leading to refinement of these methods over the past three decades (Dekker et al., 2011, Brando et al., 2009, Pe'eri et al., 2014, Sanchez-Carnero et al., 2014, Leon et al., 2013, Capo et al., 2013).

An important aspect of the application of multispectral imagery to nearshore bathymetric analysis is the temporal extent of the multispectral archive. Since the launch of the Landsat 4 in 1984, satellite imagery is available that includes reflectance information at wavelengths of particular relevance to shallow water depth analysis (blue, green, red and near-infrared wavelength ranges). Hence the archive represents a thirty year repository of nearshore information. Investigation of this record offers the potential to uncover decadal patterns of nearshore morphological change which are essential in understanding the behaviour of the subaerial shoreline (Ruggiero et al., 2005).

The morphology of the nearshore directly mediates the effects of hydraulic forcing from wave energy or tidal currents, on the subaerial beach. The presence or absence of nearshore sediment deposits such as sandbars, protect or expose coastlines to erosion from wave energy (Ruggiero et al., 2005), while changes in morphology of units such as ebb-tidal deltas cause changes to tidal currents which affect the movement of sand on and off the shoreline and directly impacts on accretion and erosion regimes on adjacent coastlines (Hansen et al., 2013, Barnard et al., 2012, Goodwin, 2014). Coastal compartment elements that exhibit high degrees of morphodynamism over multidecadal timeframes, such as ebb- tidal deltas, therefore have particular relevance for detailed coastal morphological analysis. A record of nearshore change at inter-annual to decadal timescales can contribute to greater understanding of the complexity of coastal morphological variability and inform the development of models to forecast coastal responses to variations in climatological forcing agents.

This project was designed to explore the potential of the Landsat 5 multispectral image data set to retrieve reliable nearshore topographies in order to map and analyse multi-decadal morphological variations in the ebb-tidal delta at the Wide Bay Inlet at the southern end of Fraser Island. This compartment is highly dynamic, micro-tidal, wave-energy dominated with longshore sediment transport from the south and fluctuations in wave climate between a uni-modal SE climate and a bi-modal E and SSE wave climate (Goodwin et al., 2013).

2 Literature Review

2.1 Large Scale Coastal Behaviour

Morphological variability at decadal to millennial time scales is evident in shoreline movement and beach rotations, changes in tidal inlet size and channel orientation, spit elongation and swash bar migrations, as well as large scale sedimentary cycles encompassing major storm erosion and recovery driven by oscillations in wave climate generated by prevalent atmospheric forcing mechanisms (FitzGerald and Miner, 2013, Short and Jackson, 2013). This decadal to millennial variability, identified as Large Scale Coastal Behaviour (LSCB), is particularly relevant for coastal planning as investigations into the extent, patterns and drivers of naturally occurring coastal variability at this scale can provide insights into the impact of climate change, particularly with regards to sea level increase and wave climate variation (FitzGerald et al., 2008, Short and Jackson, 2013).

Focussing on LSCB enables coastal geomorphologists to investigate the linkages between coastal morphologic dynamism and cycles of climate variation active with periodicity ranging from years to centuries (for instance ENSO, IPO, AMO, SAM). It has been argued that focusing investigations within engineering spatial and temporal parameters, (days to years), emphasises shoreline variation that is 'noise' over longer time scales (Cowell et al., 2003a, Woodroffe and Murray-Wallace, 2012, Slott et al., 2006, Dawson et al., 2009). Without the perspective of LSCB, research can overlook the ways in which coastal systems achieve equilibrium over multi-decadal time spans along coastal units linked by a common source of sediment. Figure 1 illustrates the spatial and temporal extents, along with process drivers associated with LSCB. In addition, the application of generalised coastal engineering response models such as the Bruun Rule do not adequately predict shoreline behaviour in many coastal settings due to the oversimplification of the relationships between geomorphology, sediment budget, forcing variations and antecedent environmental constraints (Hennecke and Cowell, 2000, Woodroffe and Murray-Wallace, 2012).

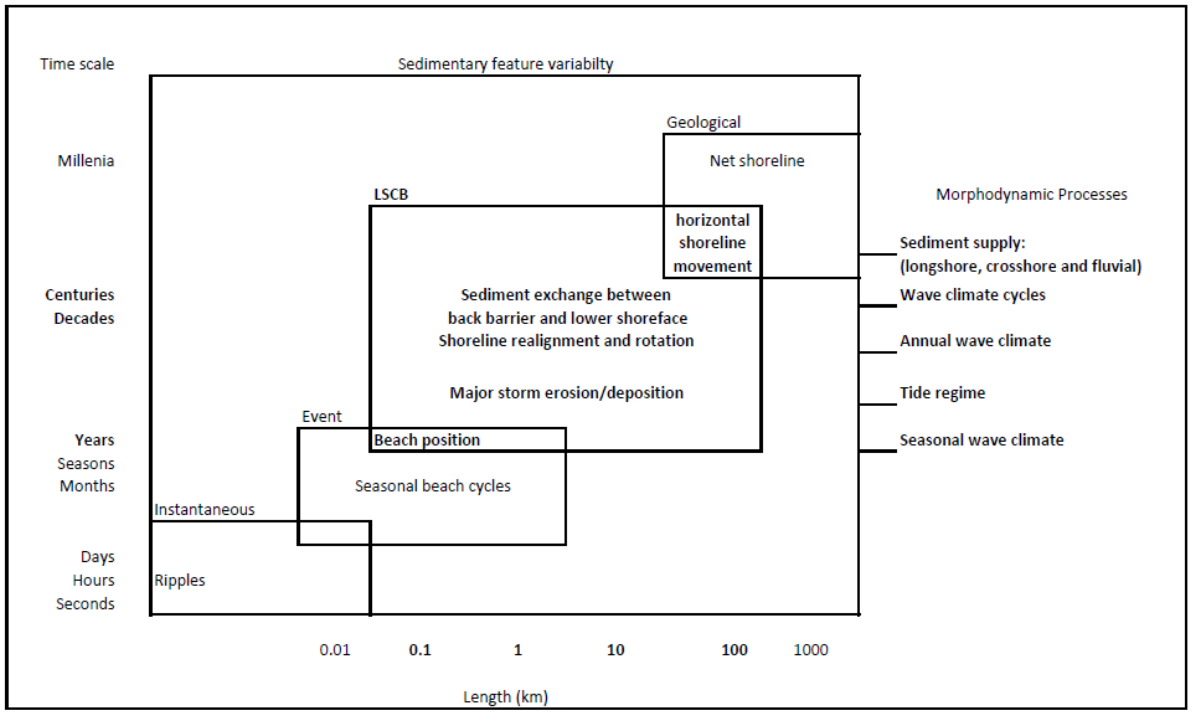

Figure 1: LSCB in relation to spatial and temporal limits, and processes driving feature variability. Diagram is a variation on *Figure 4* in Short and Jackson (2013).

Coastal morphological dynamism at LSCB spatial and temporal scales, is the result of sediment movement between the nearshore and subaerial beach and back barrier. In the case of tidal inlets this interchange is made more dynamic by the regular shifts in hydraulic forcing through ebb and flood tidal currents and variations in tidal prism (Hayes, 1980, FitzGerald and Miner, 2013). In order to develop predictive models of shoreline behaviour in the vicinity of tidal inlets, it is necessary to understand cycles of variability within the ebb-tidal delta morphology and incorporate this variability within conceptual models that are capable of describing what Wright and Thom (1977) identified as the interrelationship between short term and long term evolutionary sequences.

2.2 Conceptual models- The Coastal Tract

The 'Coastal Tract' model proposed by Cowell et al. (2003a) outlines a conceptual model that links what the authors call low- order coastal change (macro to mega scale change) to a cascading series of changes at increasingly smaller spatial and temporal scales. The tract is unified by the underlying constraint of the specific continental margin morphology and the sediment supply within the tract. Tract units dynamically interact with larger and smaller units in the cascade as sediment supply crosses thresholds which drive morphological adjustment in lower or higher units. As sediment transport is driven by waves and currents the entire

morphodynamic process is linked to the periodicity of the prevailing climate drivers. (Cowell et al., 2003a, Cowell et al., 2003b).

The Coastal Tract model emphasises contiguity between the lower and upper shoreface and backbarrier with morphological change in one forcing a corresponding change in the others. Each of these coupled elements form independent units of higher order and each is subject to morphological adaption over differing timescales with the upper shoreface most affected by synoptic or seasonal forcing agents while for the lower shoreface morphological change occurs over millennia. While the upper shoreface is subject to the highest level of morphological dynamism, the detail of emergent morphological features is dependent on the sediment supply into and within the tract, the accommodation space available in each unit and the prevailing forcing processes driving sediment exchange between the units (Cowell et al., 2003a). The Coastal Tract model hence provides a conceptual framework with which to explore the direct linkages between synoptic to inter-annual upper shoreface morphological dynamism and multi-decadal to millennial coastal variability.

Within the constraints of antecedent physiography, coastline morphology is dependent on sea level, sediment availability and wave, tide and wind energy (Thom, 1983, FitzGerald and Miner, 2013). On the SE Australian coastline sediment transport into coastal compartments and between back barrier and lower shoreface is predominantly controlled by the intensity and the direction of waves which activate longshore and cross shoreface sediment movement and the intensity and frequency of storm events. Longshore transport is driven by shore oblique wave direction while there is generally net onshore transport during periods of quiescence and net offshore transport is activated in during storm activity (Davidson-Arnott, 2011). Wave climate (direction, period and height) and storm intensity and frequency are driven by large scale climate systems and a number of studies have demonstrated that variations in wave climate can be correlated to variations in atmospheric climate indices (Goodwin, 2005, Ashton and Murray, 2006, Barnard et al., 2012, Splinter et al., 2012, Goodwin et al., 2013). Given the correlation between wave climate variation, storm intensity and climate indices, variability in coastal morphology can reflect periodic shifts in climate drivers. By identifying morphological signatures of climate forcing agents, coastal process researchers can anticipate possible future coastline change under projected climate regimes and investigate the paleo and historical geomorphic record for evidence of past climate patterns.

2.3 Tidal inlets

Returning to the conceptual model proposed by Cowell et al (2003a, 2003b), the entrainment of sediment between backbarrier, upper and lower shorefaces is driven by wave climate and storm regimes. As sediment is exchanged between each unit, morphological change will depend on accommodation space available in each unit. Change in sea level initiates an effective change in accommodation space which will initiate morphological adjustments across the tract. In stable sea level conditions where the upper shoreface experiences sediment equilibrium (static or dynamic) sediment fluxes from back barrier or lower shoreface will lead to shoreline progradation or recession (Cowell et al., 2003a). Sustained lateral movement in the shoreline position, as a lower order adjustment, will exhibit periodicity in over decades to centuries. However this movement is realised through the aggregated morphological changes within higher order elements observable over years and decades. Therefore the investigation of morphodynamism of shoreface elements, such as ebb-tidal deltas, over multi-decadal timescales gives coastal process researchers the opportunity to identify long term inherent variability within the tract. Documenting morphological change and correlating this change to increasingly detailed understandings of climate forcing variables offers the potential to use hindcast data to anticipate future responses to a range of possible forcing processes (French and Burningham, 2013).

Kraus and Kim (2009) offer the following straightforward definition of a tidal inlet – *a short narrow waterway connecting a bay, estuary or similar body of water with a larger body of water such as a sea or ocean upon which the astronomical tide acts.* While the morphology of any particular inlet is limited by the underlying geological and stratigraphic constraints, its morphological dynamism is dependent on sediment supply particularly longshore sediment transport rates and transfers through the inlet from the back barrier, the relative strength of wave energy to tidal flow, the size of the tidal prism and the wave climate and storm regimes impacting on the inlet.

The fundamental morphological units of the tidal inlet were identified by Hayes (1980) as the channel, the flood tidal delta or flood shoal, the ebb-tidal delta or ebb shoal, channel and

swash bars on the up drift side of the channel, and channel and swash bars on the down drift side of the channel (Figure 1).

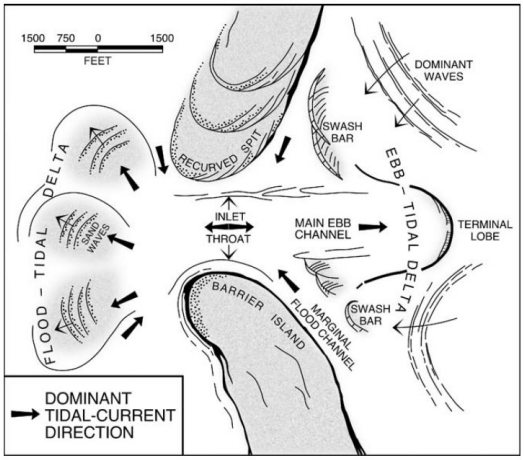

Figure 2: Morphology of Tidal inlets reproduced from Hayes and Fitzgerald (2013)

Hayes is also responsible for formulating a typology that classifies coastal compartments according to the relationship between mean tidal range and mean wave height (Figure 2). This framework remains of fundamental utility in understanding the morphodynamics of particular tidal inlet systems as it defines the dominant source of energy within an inlet system (Fitzgerald and Nummedal, 1983, Boyd et al., 1992)

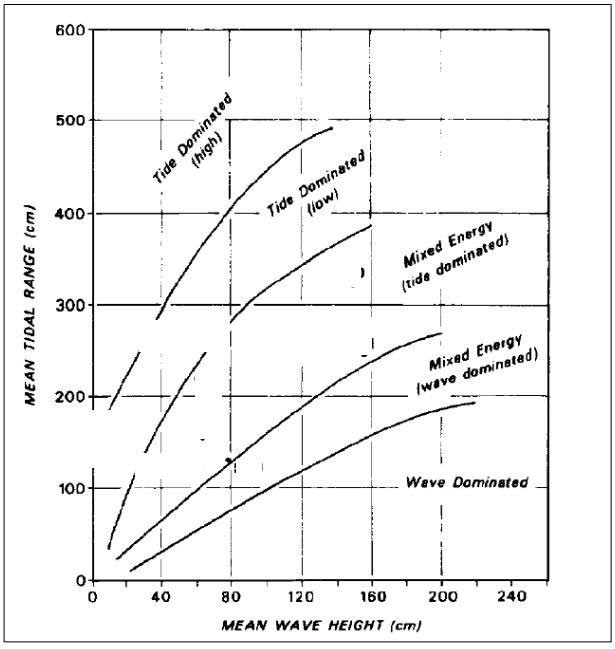

Figure 3: The Hayes framework of inlet type as a relationship between tidal range and mean wave height. After image in FitzGerald and Nummendal (1983)

Size and position of the main channel, shoals and bars evidence the directional and scalar properties of tide, wave and sediment transport acting on the inlet as well as influencing the deflection and sand bypassing processes along the outer limit of the ebb-tidal delta. Hence the ebb-tidal delta is at once partly a result of and a control on sediment transport from the up drift to the down drift side of the tidal delta.

Behaviour of these coastal elements exert first order influence on sediment availability to adjacent coastlines and the creation of swash bars and sand lobes on the upper shoreface modulate the impact of wave energy on the shoreline and in themselves evolve morphologically in relation to longshore and cross-shore forcings (Hayes, 1980, Sha, 1989, Dyer and Huntley, 1999, Kraus and Kim, 2009). In the case of ebb-tidal deltas, Fitzgerald et al (2000a), identify the governing variables of delta morphology to include tidal prism, inlet geometry, wave and tide energy, sediment supply, regional stratigraphy, slope of the nearshore, and engineering modifications. Under non-storm conditions the development of a terminal lobe of sediment at inlet mouth, creates both a redirection of longshore transport and a subaqueous unit to dissipate wave energy and create currents responsible for the migration of swash bars back onto the beaches adjacent to the inlet.

In this generalised summary of the sediment transport into and out of tidal inlets, FitzGerald et al (2000a) identify that the sediment moves into the inlet under the influence of wave or strong flood tide currents and moves out to the ebb shoal during non-storm periods. Wave shoaling and breaking at the terminal lobe of the ebb shoal generate currents which transport sediment towards the shore across the swash platform or along the edge of the terminal lobe towards inlet adjacent beaches. The magnitude of inlet sediment bypassing and the morphology of the actual ebb-tidal delta is dependent on the magnitude the longshore transport sediment supply, wave energy and incident angle and the stability of the current throat position. In addition a fundamental limiting parameter for overall ebb-tidal delta size is the tidal range and the size of the tidal prism (Sha, 1989, Kraus, 2005, Hayes and FitzGerald, 2013). Fitzgerald et al (2000) propose a number of conceptual models to demonstrate bypassing processes and the morphological signatures for variations of antecedent morphology and forcing components. Of particular relevance to this study of the Wide Bay

Ebb-tidal delta are the processes of ebb-tidal delta breaching and a subset of this model, outer channel shifting (Figure 3).

Both models relate to a stable inlet throat, and an ebb-tidal delta that is subject to significant longshore transport. These models describe the perturbation of the main ebb channel towards the down-drift shoreline, the development of extensive up-drift spits and channel lateral bars, and the eventual breaching of this bar system which isolates accumulated sediment on the down drift side of the newly aligned main channel. Morphology of the swash platform is then transformed as this sediment is transported onshore. In a previous empirical study at Prince Inlet on the South Carolina coast, Fitzgerald and Nummedal (1983), observed an ebb-tidal delta breaching cycle of between 4 and 7 years duration.

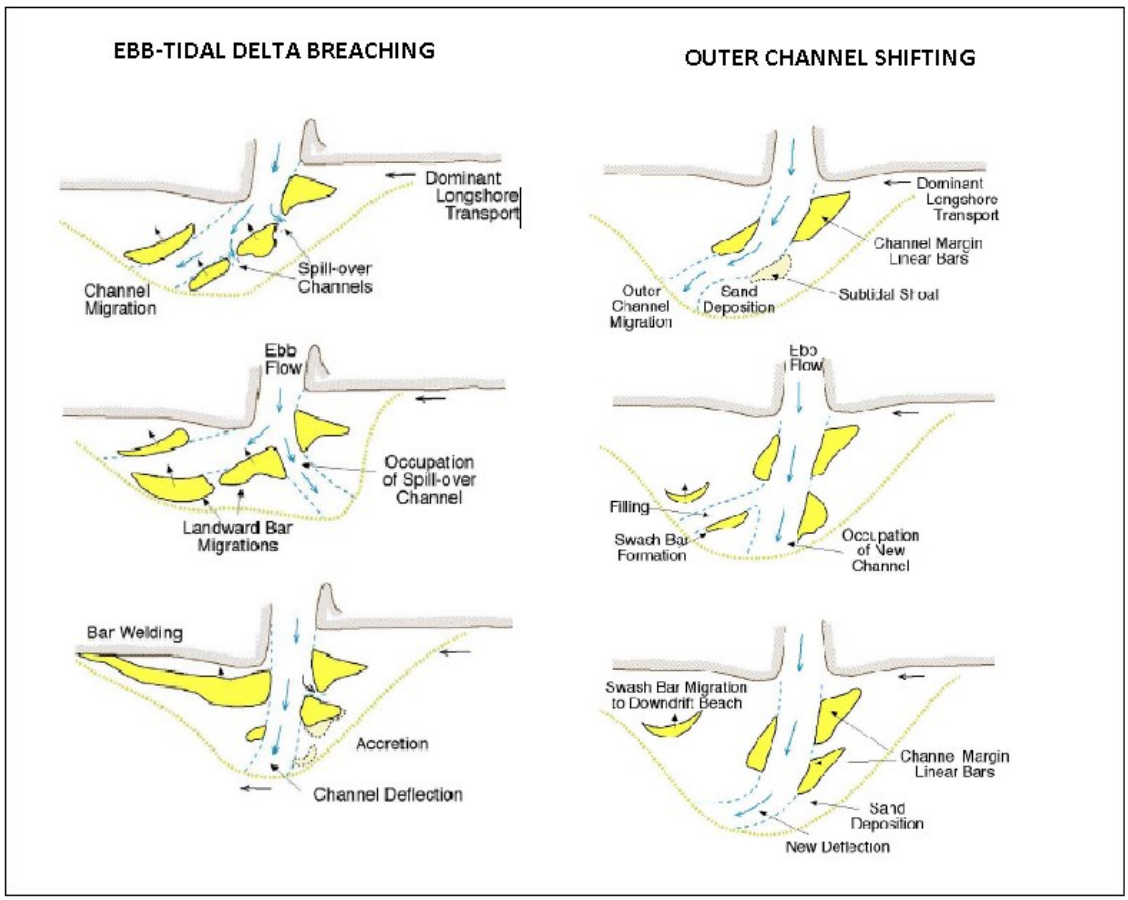

Figure 4: Conceptual models of sediment bypassing of tidal inlets and ebb-tidal delta morphological behaviour. Reproduced from Fitzgerald et al (2000)

The interrelationship between ebb-tidal delta morphology and shoreline behaviour has been studied through the use of historical hydrographic charts, maps and photography (Gaudiano and Kana, 2001, van Heteren et al., 2006, Costas and FitzGerald, 2011, Cooper et al., 2007,

O'Connor et al., 2011), and through the use of sonar or LiDAR bathymetric surveys aligned to terrestrial shoreline data (Vinther et al., 2004, Morgan et al., 2011, Barnard et al., 2012, Hansen et al., 2013). With the release of large multispectral satellite image archives (Landsat and SPOT), time series analysis of inlet morphology across multidecadal sequences is also being investigated (Capo et al., 2013).

Changes in inlet morphology can have significant economic ramifications as commercial shipping between backbarrier harbours and open water depends on the inlet channel being navigable (Kraus and Kim, 2009). In addition, the effects of ebb-tidal delta morphodynamism on adjacent shorelines can lead to significant coastline recession and impact on valuable infrastructure. Interventions at inlets such as jetty construction, channel dredging and adjacent beach nourishment have all resulted in sometimes unanticipated and unwelcome shoreline responses which have highlighted inadequacies in theoretical understanding of the mechanics of sediment movements in inlet systems (Kraus, 2005, Beck and Kraus, 2011, Brayshaw and Lemckert, 2012, Castelle et al., 2007, Liria et al., 2009). Hence continuing investigation into tidal inlet morphodynamism and behaviour of ebb-tidal deltas remains of fundamental importance to understanding how a sedimentary coast responds to variations in forcing agents, natural or anthropogenic.

As already mentioned, over the past four decades much research has focussed on the identification of tidal inlet constituents, defining boundary conditions in order to create typologies and conceptual models and empirical studies of particular ebb-tidal delta variability over the historical record (Kana et al., 1999, Boyd et al., 1992, van Heteren et al., 2006, Costas and FitzGerald, 2011, Seminack and Buynevich, 2013). In addition the development of predicative and hindcasting models of delta behaviour has been informed by hydrodynamic principles and fluid mechanics (Bertin et al., 2009, Dissanayake et al., 2009, Dodet et al., 2013, Kraus, 2005).

The major insights informing this research project into the Wide Bay ebb-tidal delta can be summarised as follows:

- In mixed energy (wave dominated environments) the ebb-tidal delta will be less extensive than those in tide dominated deltas and the depth of the ebb delta terminal lobe will be constrained to the depth of closure defined by storm wave height (Hayes, 1980, Kana et al., 2011).
- If the ebb-tidal delta is subject to significant longshore currents and sediment transport, the position of the main channel can be expected to be perturbed in the down drift direction, leading to an extensive up-drift attached bar which will eventually lead to hydraulic inefficiency resulting in shoal breaching and reorientation of the main channel.(FitzGerald et al., 2000a)
- Delta breaching instigates major events of sediment bypassing the inlet. Movement of this sediment across the swash platform is dependent on incident wave climate. Location of bar attachment to shoreline may result in reversal of LST currents on the shoreline between attached bar and inlet , strengthening flood currents leading to shore recession and sediment redirection back into the delta (Sha, 1989, Dyer and Huntley, 1999).
- Major bar attachment events deflate the swash platform and reduce overall volume of ebb-tidal delta leaving shoreline subject to greater wave energy. Rates of regrowth of the ebb delta, dependent on sediment supply, tidal prism and wave climate (FitzGerald et al., 2000a).
- Channel bedforms and swash bar orientation reflect dominant forcing agent- tidal currents or wave generated currents- long shore and across swash platform (FitzGerald and Miner, 2013).

2.4 Application of optical satellite imagery to near shore depth retrieval

Detailed observation study of nearshore topography has been hampered by the difficulties in surveying shallow nearshore waters. Sonar and acoustic sounding methods are limited to depths able to be accessed by relatively large vessels and aircraft mounted LiDAR sensors have not, until recently, been able to deliver accurate measurements in shallow water environments (Lyzenga et al., 2006, Gao, 2009, Leon et al., 2013). This situation has changed dramatically with the development of LiDAR scanning methods suited to shallow water depth

retrieval with the development of sensors utilising multiple lasers with green and infrared bandwidths and full waveform recording to enable more accurate discrimination of surface and seabed returns. The public release of multidecadal multispectral satellite data sets (Landsat and SPOT) suitable for optically shallow water depth analysis has also created new opportunities for nearshore bathymetric determination. The Landsat multispectral satellite imagery archive is an important resource for coastal process researchers, holding almost four decades of imagery which enables detailed time series analysis of coastline variability.

Investigating bathymetric surfaces using multispectral optical satellite imagery relies on the application of the principles of light transmission in water (Gao, 2009). Shallow water reflectance models can be utilised with optical satellite imagery to derive depth measurements from reflectance values after atmospheric and water column absorption, scattering and attenuating factors are taken into account.

Optical satellite imagery, both multi and hyperspectral, is a form of passive remote sensing that records the reflectance of solar electromagnetic radiation from intercepting surfaces back to platform sensors. Reflectance values received at sensor are the result of absorption, refraction and reflection as light passes through the atmosphere, and any other medium such as water, and interaction with reflecting surfaces (Mather and Koch, 2011). Optical sensors typically record reflectance values for wavelengths in distinctive bands from the approximately 400nm through to the infrared range up to approximately 2300nm. Because wavelengths above 750nm are mostly absorbed by water with little reflectance, bands in the visible spectrum 400nm to 650nm wavelengths are utilized in bathymetric analysis.

Shallow water reflectance models can be utilised with optical satellite imagery to derive depth measurements from reflectance values after atmospheric and water column absorption, scattering and attenuating factors are taken into account. However as each of these input parameters varies according to time and location, developing models that can reliably detect depth and therefore benthic morphology, has challenged researchers for the four decades that optical satellite imagery has been available. Recent developments in the field, while optimising new technologies and sensor capabilities, still utilise two fundamental approaches to isolating the depth component of reflectance values: either analytical models which

although theoretically robust, are complex and require a number of in situ measurements, or empirical models which although less complex can still produce reliable information in specific circumstances (Gao, 2009).

Deriving bathymetric information from optical satellite data is based on the principle expressed by Beer's Law that there is an exponential relationship between the attenuation of light in water and the depth of the water column (Stumpf et al., 2003). As well as attenuation due to depth, reflectance values in water are affected by the albedo of the substrate and material suspended in the water column (Bierwirth et al., 1993, Maritorena et al., 1994). In a seminal work that has informed linear analytic models of water column analysis, Lyzenga (1978) developed an algorithm expressing the exponential relationship between reflectance (R_w) and depth (z), and the linear relationship to bottom albedo (A_d):

$$R_w = (A_d - R_\infty)\exp(-gz) + R_\infty$$

where R_∞ represents reflectance values from optically deep water (i.e. no interaction with substrate) and g is a function of the attenuation of downwelling and upwelling light due to water column constituents locally measured.

The limitations of a single wavelength (or band as per sensor calibration) solution for this algorithm, are such that it cannot resolve depth over an area if substrate, and therefore albedo, is not constant nor if water column constituents vary markedly. Lyzenga proposed using two bands as a correction to albedo variation so that the linear relationship of bottom albedo could be separated from the exponential attenuation due to depth. This solution however still required tuning with site specific derivations of attenuation coefficients for water column constituents and deep water reflectance, which complicates the application of the method to extensive or remote sites (Maritorena et al., 1994, Lee et al., 1999). The assumption of uniform substrate albedo and homogenous water column constituents can also introduce significant inaccuracies in identifying the depth component of the reflectance values and addressing this limitation continues to present challenges for contemporary researchers (Su et al., 2014, Ma et al., 2014, Sanchez-Carnero et al., 2014, Kanno et al., 2013).

While analytical models are theoretically robust, the need for multiple in situ derived tuning coefficients (or highly complex in-image derivation) limited the utility of the model for remote areas readily imaged by satellite sensors, but without readily available site specific in situ data.

To overcome these limitations, Stumpf et al (2003) developed an alternative algorithm based on the ratio of the log of reflectance values between two bands or wavelengths. The method utilises differential wavelength-dependent attenuation rates to overcome the potential interference from varying substrate albedo. Because the attenuation rate due to depth is exponential, reflectance values will decrease more quickly at higher absorbing wavelengths compared to lower absorbing wavelengths. By comparing a log transform of these values a linear relationship between the attenuation rates is established and depth could be inferred from ratio values. The algorithm as published in the 2003 paper does include tuning coefficients (m_1, m_0, n) to establish actual depth, but relative depth values can be derived without these coefficients ($Z = \text{depth};\ R_w(\lambda_i) = \text{reflectance at wavelength } i$) :

$$Z = m_1 \frac{\ln(nR_w(\lambda_i))}{\ln(nR_w(\lambda_j))} - m_0$$

As with the linear algorithm proposed by Lyzengar, water column properties are assumed to be homogenous, which can be problematic as the inherent optical properties (IOPs) of the water column- for instance chlorophyll content or coloured dissolved matter- can profoundly affect reflectance values (Maritorena et al., 1994). Hence while both the linear and ratio transform algorithms can be solved for depth, the accuracy of the resultant depth findings can be confounded by spatial variability in both substrate and IOP which do not adhere to assumptions of homogeneity in each model. Much research in the application of optical remote sensing has focussed on how to develop analytic or empirical models to improve accuracy and reliability of depth prediction, and identify wavelengths most suited to retrieve reliable depth measurements in turbid as opposed to clear water environments (Dekker et al., 2011, Sanchez-Carnero et al., 2014).

In a comparison of five commonly used methods of shallow water mapping using optical satellite imagery, one empirical and four analytic, Dekker et al (2011) come to the following conclusions about the relative merits of each methodological approach:

1. Analytic models are more accurate then empirical models for bathymetric retrieval, but are much more complex requiring substantially longer processing time
2. Both approaches produced moderately accurate retrievals to a depth of approximately 13 metres

3. The analytic models that incorporated in situ data variables were the most accurate but could not be of use in areas where such in situ data was not available

While Dekker et al (2011) provide extensive discussion of analytic models which produce retrievals with high accuracy, the authors still conclude that for regions where in situ data collection is not possible or unavailable, empirically based methods can provide reasonable estimates of bathymetry in regions of relatively homogenous bottom albedo and within the depth limits of optically shallow water. This finding is particularly relevant in the use of historical imagery as obtaining in situ water column data is generally impossible for data collected in the past.

Generally optical sensor depth retrieval research has focussed on the following aspects of optical sensor methods:

- examining the effects of variations in substrate albedo and water column properties (Lee et al., 2012, Collin and Hench, 2012)
- comparing results of different wavelengths used in the algorithms (Sanchez-Carnero et al., 2014, Doxani et al., 2012)
- extending reflectance analysis with hyperspectral imagery (Su et al., 2014, Ma et al., 2014)

As stated previously, methods based on assumptions of homogeneity of substrate and inherent water properties did not match the reality of many coastal environments in which depth analysis would be implemented (Maritorena et al., 1994, Stumpf et al., 2003). Lee et al (1999) developed a physics based semi-analytic method to simultaneously derive both water depth and water column properties which has informed the development of many semi-analytic methods, such as the four methods discussed in the Dekker et al (2011) review. The capacity to derive depth values directly from image data, without the necessity for in situ tuning is a major focus research using these models particularly in relation to hyperspectral imagery (Lee et al., 2007, Brando et al., 2009). Comparison of image derived bathymetries to LiDAR or in situ depths show error averages for the derived depths of between 10 and 15% for depths to 25 m (Brando et al., 2009, Lee et al., 2007).

However as noted by Dekker et al (2011) and Gao (2009), semi-analytic methods are complex and require sophisticated processing for the degree of accuracy they deliver and using the simpler linear inversion or ratio transform models may produce useful results. Dekker et al (2011) caution that application of any of the inversion algorithms is predicated on recognising known depth limitations of the algorithm and any confounding factors due to heterogeneity of substrate and IOP. Both depth limitations and interaction with IOPs are dependent on the behaviour and transmission of particular wavelengths in the water column, so that choice of bands to be used in the model fundamentally affect the functionality of the result. Comparisons of the performance of different spectral bands in both linear and ratio transform algorithms has been an important aspect of shallow water depth investigation which has developed as new generation sensors with extended spectral ranges have been operationalised.

Selection of band or wavelength for inclusion in calculations is dependent on the water penetrating capacity of the wavelength. Wavelengths in the blue and green range of the visible spectrum have the strongest water penetration capabilities (Gao, 2009) and have been used since the earliest investigations of shallow water depth analysis (Lyzenga, 1978, Bierwirth et al., 1993, Maritorena et al., 1994). Stumpf et al (2003) utilized bands in the blue and green spectral range implementing their Ratio Transform algorithm. While blue and green sections of the optical spectrum have the strongest water penetration capabilities, reflectance of longer wavelengths in the red and NIR range are can be utilised to generate masks over land masses in imagery (NIR wavelengths), and generate IOP coefficients of water bodies, as the green to the NIR wavelengths are sensitive to organic particles and dissolved coloured matter within the water column (Mather and Koch, 2011). Band selection is also contingent upon the sensor capabilities of the satellite platforms employed. The earliest multispectral Landsat sensors launched in 1972 consisted of a four band instrument with two bands in the visible spectrum (green and red) and two NIR channels. In 1982 the number of bands was increased to seven with the launch of the Landsat 4 TM sensor which included a band in the blue spectral range and channels in the thermal infrared range. The most recent Landsat 8 mission (2012) includes sensors tuned to shorter blue wavelengths (Coastal blue). Other multispectral platforms include SPOT (launched 1986), SeaWiFS (launched 1997), IKONOS (launched 1999),

MODIS (launched 1999), MERIS (launched 2002) and Worldview 2 (launched 2009). The number of bands and bandwidths vary from platform to platform as does spatial and radiometric resolution (Mather and Koch, 2011).

Lyzenga's algorithm and Stumpf's Ratio Transform algorithm were developed and implemented using wavelengths in blue and green spectral bands (Lyzenga, 1978, Lyzenga et al., 2006, Stumpf et al., 2003). Both algorithms are based on assumptions of a homogenous substrate and relatively clear water column. However for coastal waters with greater amounts of suspended sediment or organic matter, longer wavelengths in the green band, with reflectance influenced by IOPs, have been incorporated into the linear algorithm with promising results. In a study of the Mediterranean Greek coast, Doxani et al (2012) spatially sub-set a high resolution Worldview 2 multispectral image into homogenous benthos types then applied the Linear model to the visible and NIR band reflectance in each region, and concluded that the green band was the most effective for bathymetric applications.

The Doxani et al study (2012) also found that the yellow and red bands reflectance were significant in areas of seagrass substrate, which accords with the findings of Burns et al (2010) in investigation of Moreton Bay on the SE Queensland Coast. Utilising Hyperion hyperspectral data, reflectance in the blue (460nm), green (550nm) and the red (650nm) wavelengths were incorporated in the Linear algorithm then log transformed to include in the Lyzenga log ratio. The reflectance values for the blue and green bands were incorporated directly into the Stumpf Ratio Transform equation. The authors found that the Lyzenga model incorporating green and red bands in the linear then ratio algorithms produced depth predictions with one tenth of the error of the simple green band linear transform, and could not find any sensitivity to depth using the Ratio Transform as described by Stumpf et al. The authors state that this may be related to the specific shallow water properties for which the Ratio Transform was developed, that is coral reef environments (Burns et al., 2010).

However other recent studies suggest that the Ratio Transform algorithm remains valid in tropical coral reef waters and may have novel possibilities utilising multiple angle multispectral data and hyperspectral reflectance signatures. Collin and Hench (2012), in a reef study in Moorea, French Polynesia found that the Ratio Transform algorithm applied to

Worldview 2 coastal blue, green, yellow and NIR bands was able to produce depth models that were sensitive to 30 metres, which increases by 10 metres the generally accepted limits of optical depth detection. Lee et al (2012) used nadir and non-nadir Worldview 2 images to investigate view angle and a green/yellow band Ratio Transform but again found that the absolute depth determination may be confounded by the high albedo sand substrate. Ma et al (2014) use the full spectral signature derived from each pixel in hyperspectral Hyperion imagery to first match for spectral similarity then use this coefficient in the Ratio Transform equation to develop relative depth models. While their study is preliminary they claim that their results show promise in waters less than 20 metres, and is utilising the density of spectral data available in hyperspectral data sets.

While absolute depth retrieval is vital for the production of navigational charts or studies of nearshore ecotones, retrieval of relative depth surfaces may still afford coastal geomorpholgists important information on the structural and sedimentary units of the near shore. In a study of a tidal inlet compartment, Sanchez-Carnero et al (2014) were able to document, using a time sequence of images, the formation of and progression shoreward of ebb-tidal swash bars. Although absolute depth retrieval error (RMSE between .33 and 1.22m to depths of 6 metres) did not satisfy navigational accuracy standards as defined by the International Hydrographic Office, the authors emphasise the significance of documenting the sediment movement in understanding the behaviour of this compartment under various climatic forcings (Sanchez-Carnero et al., 2014). An earlier study by Hu (2008) was able to document the size, extent and orientation of previously undocumented sand ridge units off the West Florida coast. This research utilised multispectral optical imagery (MODIS satellite), without resolving for absolute depth, to extract spectral data in the blue/green range, to generate images which clearly displayed benthic morphology.

While the absolute depth accuracies of satellite derived bathymetries are inadequate for reliable navigational chart development, it has been proposed by Pe'eri et al. (2014) that multispectral imagery-derived bathymetry provides a cost effective tool for the assessing navigational chart accuracy. This research was explicitly focussed on developing a methodology that could provide hydrographic offices in developing nations with the means to assess the adequacy of their records. It evaluated data, tools and algorithms that are readily

or publically available such as the USGS Landsat archive, commercially off the shelf data processing platforms (ESRI Arc GIS) and the Stumpf et al. (2003) Ratio Transform algorithm. The authors concluded that their methodology was an effective reconnaissance tool for investigating coast areas before the conducting high resolution hydrographic surveys. The derived absolute depth values as correlated to existing navigation charts, was found to be within 2m for most of the surveyed areas (R^2 =0.83) , and the greatest impact on correlation values were areas of turbidity in the imagery (very shallow surf affected areas, or sediment plumes) as well as waters beyond the depth of extinction (optically deep waters where there is no interaction with the substrate).

The Pe'eri et al. (2014) methodology informed a workflow incorporated into an International Hydrographic Organisation publication on satellite derived bathymetry (IHO, 2013). This workflow includes image pre-processing, but does not recommend radiometric and atmospheric correction as the use of the Stumpf et al. (2003) Ratio Transform algorithm is applicable to raw digital number (DN) reflectance values recorded at sensor for within-image relative depth derivation. This workflow was adopted to explore the nearshore topography of the Wide Bay Ebb-tidal delta and will be explained in more detail in the methodology section of this report. Whist derived relative depth values based on DN cannot be compared between images if individual relative depth images are each calibrated to known depth values, these individually calibrated images then can be compared .

3 Chapter 3- Site description

The tidal inlet at the southern end of the Great Sandy Strait in SE Queensland (25.828655°S, 153.067349°E), links the southern end of Wide Bay to the Pacific Ocean. It is at the northern extreme of the 1500km northerly longshore transport current extending from the Sydney Basin, which transports approximately 500,000m^3 of sand annually along the SE Queensland coast (Boyd et al., 2008). The area has a maximum tidal range of 1.78m at mean high water springs (2014), tides are semi-diurnal and coastline behaviour has been liked to variations in dominant modal wave direction and the modes of climate variability in the Southern Hemisphere, including the Southern Oscillation Index (SOI), and the Interdecadal Pacific Oscillation (IPO) (Roy et al., 2001, Goodwin et al., 2013). The wave climate for the proximate Northern NSW coastline has been shown by Goodwin et al to have two predominant modes, a uni-modal SE climate and a bi-modal E and SSE wave climate (2013). It is expected that variations in the ebb tide delta at Wide Bay will display the morphological signatures of these wave climates. The inlet is unengineered and so variation in morphology can be understood as resultant from atmospheric and oceanic forcing processes.

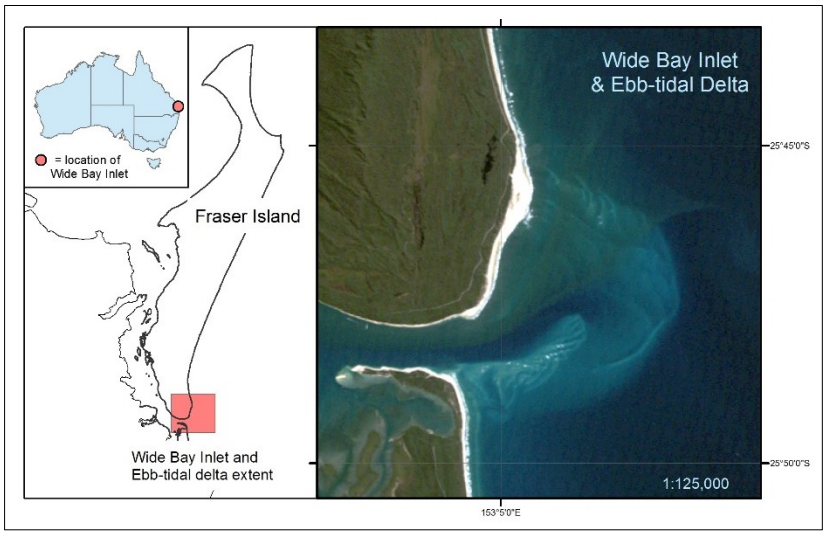

Figure 5: Location of study area: Wide Bay Inlet separates Fraser Island from the Australian mainland off the SE Queensland Coast. The ebb-tidal delta is evident in the RGB Landsat image captured on August 6 2009

4 Chapter 4 Methodology

4.1 Data

4.1.1 Landsat data

Landsat 5 and 7 data were chosen to conduct this study, because of the length of the archive for the investigation site - data is available from 1987 to 2012. Appendix 1 contains the full list of data sets used in this project. All data sets were downloaded as Level 1T processed which provides for systematic radiometric accuracy and geometric accuracy. The data is provided in a GeoTIFF format at 30 meter resolution with a UTM map projection and WGS 84 datum (USGS, 2014). Landsat imagery is freely available from the United States Geological Survey websites listed in Appendix 1.

The Thematic Mapper sensor (Landsat 5) and Enhanced Thematic Mapper sensor (Landsat 7) collected data in seven and eight spectral ranges respectively. The bands of relevance to this project are the same for each sensor:

Band 1 - 0.45-0.52µm wavelength – visible 'blue'
Band 2 - 0.52-0.60µm wavelength – visible 'green'
Band 3 – 0.63-0.96µm wavelength – visible 'red'
Band 4 – 0.76-0.90µm wavelength – near infrared

Bands 1 and 2 were included in the Ratio transform algorithm, while Band 4 was used to create a land mask and correct for sun glint. Bands 1, 2 and 3 were used to generate natural colour images.

Images were selected which contained less than 10% cloud cover according to the USGS online filter and were visually inspected on-line for evidence of sediment plume or surface turbulence which could interfere with the depth retrieval. Between 1999 and 2003 Landsat 7 ETM images were used as the Landsat 5 TM sensor images of relevant quality were not available.

4.1.2 Hydrographic charts

Seven hydrographic survey charts taken between 1868 and 1985, obtained from the Queensland State Archives and the 2009 Maritime Safety Queensland Boating Safety Chart for Great Sandy Strait South, were digitised and georeferenced to projected coordinate GDA MGA94, using ESRI ArcMap 10.1 software. Using the depth contours detailed on the charts, layers showing 1, 2 and 5 fathom contours were created. The 1985 and 2007 chart soundings are in metres not fathoms so the 2, 5 and 10 metre depth contours were used to create the relevant shape files. Appendix 2 contains details of the chart identification in the Queensland State archive holdings and corrections between charts to a common datum. Soundings from the 2009 Maritime Safety Chart (MSQ, 2009) were digitised and used to derive absolute depth values for the 2009 Landsat relative depth surface and to derive correlation and RMSE values for this set.

4.1.3 Software GIS

All data sets were processed and analysed using ESRI ArcMap 10.1 & 10.2 GIS software.

4.2 The IHO-IOC workflow-

4.2.1 Theoretic underpinnings

As discussed previously, research undertaken by Pe'eri et al. (2014) to develop practical and cost-effective procedures for deriving bathymetric estimates using multispectral satellite imagery concluded the Stumpf et al. (2003) algorithm applied to blue and green bands of images that had less than 10% cloud cover and sunglint removed returned good correlation between the algorithm results and charted water depths (R^2 =0.80-0.85). The authors note that high turbidity due to sediment content or shoreline wave action limited accuracy at depths less than 1m and in waters of any depth with increased suspended particulates. However the method was able to derive consistently reasonable depth estimation with R^2 values of between 0.80 and 0.85 for the study sites, and absolute variation between derived and measured depth of less than 2m. Depth of extinction varied across test sites from 6m to 25m.

This research informed and is the recommended methodology incorporated into a resource developed by the International Hydrographic Organisation (IHO) and the Intergovernmental Oceanographic Commission (IOC), *The IHO-IOC GEBCO Cook Book* (IHO, 2013), as a scientifically rigorous method for bathymetric estimation, though not adequate for IHO survey standards. On the basis that absolute depth to survey standard is not necessary for morphological study, the procedure outlined in the above publication was adopted to derive digital terrain models the Wide Bay ebb-tidal delta.

4.2.2 Workflow steps

The key steps of *The IHO-IOC GEBCO Cook Book* (IHO, 2013) are:

1. Image selection and pre-processing
2. Water separation
3. Spatial filtering
4. Glint/cloud removal
5. Application of bathymetry algorithm
6. Identification of the depth of extinction
7. Vertical referencing

The first five of these steps were implemented as follows

1. Image selection and pre-processing

Landsat TM or ETM images from WRS Path 89, Row 78 with less than 10% cloud cover for each year from 1987 to 2009 were selected and downloaded from USGS Glovis portal. Each image was clipped to the study area extent of Wide Bay Inlet, images were co-referenced then projected from WGS94 to map projection GDA94MGA.

2. Water separation

Band 4 (NIR - 0.76-0.90µm) of each image was used to identify the land/water boundary. As NIR wavelengths are almost complete absorbed by water, the breakpoint between land and water is evident in this band and can be used to create a mask to apply to the Band 1 and 2 images to isolate the water extent in each image. Pixel values at the intersection between the land and water were examined via examination of profile graphs of transects from land to sea.

Pixel value dramatically decreases at the land water interface and the value derived from each image was used to generate a land mask to isolate only water values in the target scene

3. Spatial filtering :

A low pass filter is applied to each band to smooth the data and reduce the effect of anomalous pixel values – ie reduce 'noise'.

4. Sun glint /cloud correction:

The sun glint correction method is as described by Hedley et al. (2005),

   a. Determine NIR band minimum brightness over deep water
   b. Perform linear regression of NIR brightness against band signal of Bands 1 and 2 to derive slope for each regression line.
   c. Deglint Band 1 and 2 images by subtracting the product of the slope and the NIR brightness of each pixel form the band pixel value.

5. Algorithm application:

The Stumpf et al. (2003) algorithm, without tuning coefficients, was applied to the glint corrected Band 1 and 2 images to derive relative depth values.

$$relative\ depth\ value = \frac{\ln(band\ 1)}{\ln(band\ 2)}$$

The ArcMap 10.23 modelbuilder workflows for these stages of processing are included in Appendix 3. Steps 6 and 7 of the IHO method were modified in order to enable comparison between the data for each year, and assess morphological change on the ebb-tidal delta.

6. Identification of the depth of extinction :

Chart sounding across the Wide Bay inlet and ebb-tidal delta were digitised from the 2009 Maritime Safety Queensland Boating Safety Chart for Great Sandy Strait South (figure 5). The relative depth values for the 2009 Landsat image (LT50890782009234ASA0) for these points were extracted and correlation explored through linear regression plotting. This dataset was randomly subset into a 112 member training set and 56 member test set derive RMSE values.

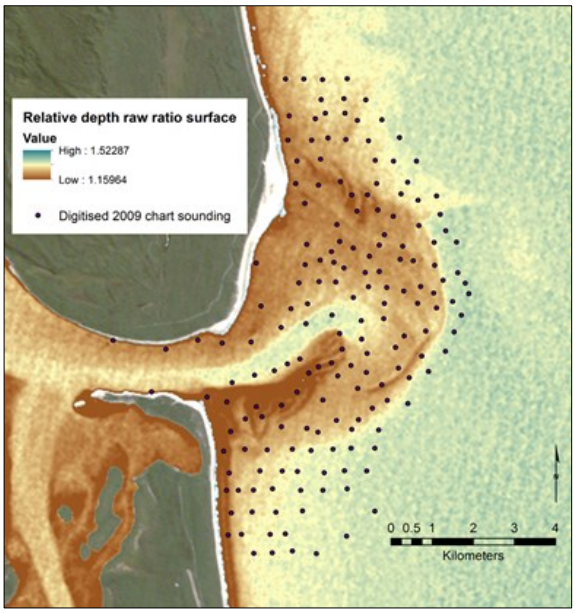

Figure 6: Location of chart soundings and relative depth value surface for 2009 image

7. Vertical referencing to chart soundings:

As concurrent verifiable depth recordings are not available for the other years in the study, the decision was made to classify relative depth values for each image, using the values derived for the 10m terminal lobe contour as the upper limit of derived depth. Consideration of the historical bathymetric survey revealed that this contour was relatively stable over the century and a half spanned by the survey data.

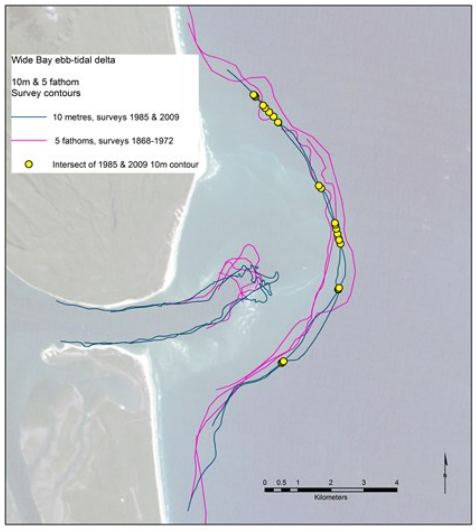

Figure 7: Location of static depth values of 10m LAT used to define limit of relative depth value included in delta analysis

To refine the region of the terminal lobe used to choose relative depth values that would be used to restrict the classification of the remaining values, a spatial intersect was performed using the 10m terminal lobe contours from the 1985 and 2009 hydrographic charts. The resultant sections of the 10m depth were used to extract relative depth values from each relative depth data set to serve as the deepest limit of the classification for that image. Hence all datasets were referenced to the area of the ebb-tidal delta most likely to be a stable and consistent sounding.

4.3 Correction to common datum (LAT)

In order to compare ebb-tidal delta morphology between years the relative depth images were tide corrected using the LAT 10m chart datum. Observed hourly water levels from the Mooloolaba tide gauge were obtained from Maritime Safety Queensland (Queensland, 2013) The Mooloolaba LAT datum is 17mm higher than the Waddy Point datum, which is the relevant datum to the ebb tide delta (2014). The observed tide value was increased by this amount to correct to the expected levels on the Wide Bay ebb-tidal delta. Observed tide levels at time of image capture were added to the 10m LAT value of the reference points, an equal interval classification performed dividing the RD values into intervals representing 0.5m segments. The resultant surfaces were then reduced to LAT by reclassing the data into 20 classes referenced from the terminal lobe 10m contour value. Appendix 4 contains recorded levels and correction calculations.

4.4 Derived data

From the primary data set of relative depth digital terrain surfaces for each year the following surfaces and datasets were derived:

1. Depth contours at 0.5m intervals for each image
2. Digital terrain models of difference generated by map algebra calculation of difference in classified depth value for consecutive years
3. Derived surfaces resultant of inter-year computation of cell statistics. All relative depth surfaces were included in analysis for minimum, maximum, mean, majority and range values for each cell. Following from the methodology of Mitasova et al. (2010) the maximum depth surface can be understood as the core surface

below which sediment is stationary and the minimum depth surface is the envelop below which all vertical and horizontal movement of sediment occurs. The majority surface indicates the level below which sediment movement is less likely further refining the depth of most sediment movement. Range surfaces highlight the spatial extent of depth variation.

4. Profiles of relative depth surfaces and statistical surfaces along transects across morphologically significant element of the ebb-tidal delta: the up-drift and down-drift channel linear bars, main ebb channel, swash platform bar welding regions and main ebb channel cross section.
5. Spatial and relative volumetric change analysis of the ebb-tidal delta as a whole, and also sectioned to up-drift and down-drift portions based on the mean position of the main ebb channel midline. Area was calculated as the product of pixel count by $900m^2$ (the pixel size being 30 x 30m); volumetric change was derived from the depth difference surfaces values multiplied by area; comparison between years was by means of a running total of the relative volumetric change for consecutive years.

5 Chapter 5 – Results

5.1 Validation

5.1.1 Linear Regression

Figure 7 displays the linear regression graph for the 2009 image relative depth values with 2009 chart soundings, showing the derived R^2 value of 0.76 comparing favourably to the Pe'eri et al. (2014) R^2 value between 0.80 and 0.85

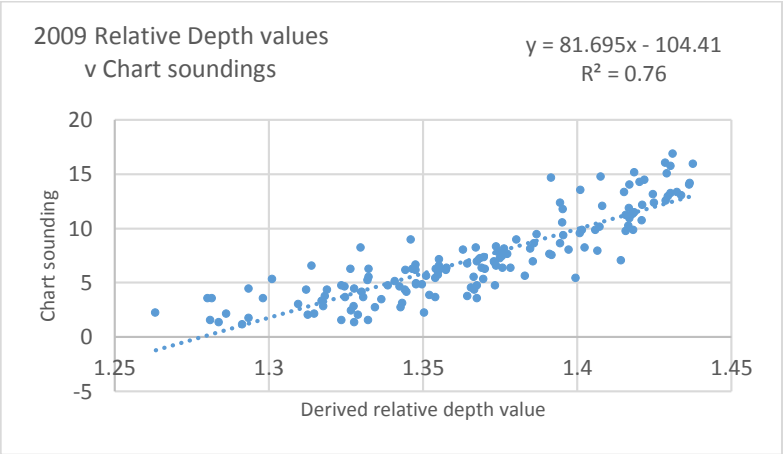

Figure 8: Linear regression of 2009 relative depth values and 2009 chart soundings including R^2 value.

5.1.2 RMSE analysis

RMSE analysis was conducted by randomly subsetting the data set into a 112 member training subset and a 56 member test subset. Figure 8 shows the result of the regression analysis for the training subset

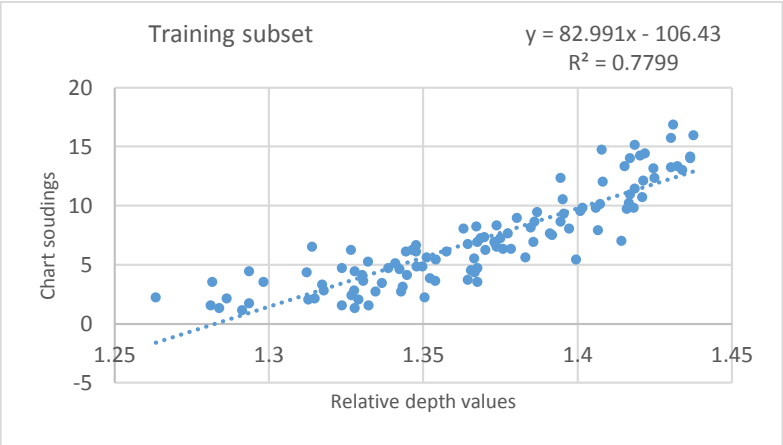

Figure 9: Linear regression on 112 member training subset

Table 1: RMSE calculation for test subset of 2009 soundings/Relative depth value

Relative Depth value	*Sounding*	*Predicted Depth*	*Difference*	*Relative Depth value*	*Sounding*	*Predicted Depth*	*Difference*	*Relative Depth value*	*Sounding*	*Predicted Depth*	*Difference*
1.2815	2.8	-0.0736	-2.8736	1.3696	5.3	7.2340	1.9340	1.4038	8.5	10.0752	1.5752
1.3097	3.0	2.2596	-0.7404	1.3324	5.5	4.1495	-1.3505	1.3461	8.9	5.2859	-3.6141
1.3075	3.1	2.0802	-1.0198	1.3549	5.7	6.0111	0.3111	1.4088	9.2	10.4916	1.2916
1.2801	3.5	-0.1906	-3.6906	1.3565	5.8	6.1499	0.3499	1.3907	9.3	8.9822	-0.3178
1.3249	3.6	3.5239	-0.0761	1.3553	6.1	6.0479	-0.0521	1.4116	10.0	10.7218	0.7218
1.3183	3.7	2.9753	-0.7247	1.3542	6.2	5.9559	-0.2441	1.4082	10.2	10.4342	0.2342
1.3441	3.8	5.1179	1.3179	1.3325	6.2	4.1562	-2.0438	1.4159	11.2	11.0753	-0.1247
1.3426	4.2	4.9925	0.7925	1.3692	6.3	7.1985	0.8985	1.4180	11.3	11.2551	-0.0449
1.3190	4.3	3.0340	-1.2660	1.3578	6.3	6.2521	-0.0479	1.3954	11.7	9.3754	-2.3246
1.3441	4.3	5.1213	0.8213	1.3367	6.3	4.5062	-1.7938	1.4169	11.8	11.1584	-0.6416
1.3624	4.3	6.6339	2.3339	1.3553	6.5	6.0484	-0.4516	1.4350	12.4	12.6613	0.2613
1.3657	4.3	6.9146	2.6146	1.4037	6.7	10.0626	3.3626	1.4289	12.5	12.1531	-0.3469
1.3447	4.5	5.1655	0.6655	1.3552	7.1	6.0387	-1.0613	1.4294	12.9	12.1980	-0.7020
1.3511	4.5	5.7021	1.2021	1.3756	7.4	7.7336	0.3336	1.4011	13.5	9.8474	-3.6526
1.3246	4.6	3.4997	-1.1003	1.3743	7.8	7.6230	-0.1770	1.3915	14.6	9.0546	-5.5454
1.3735	4.7	7.5576	2.8576	1.3764	8.1	7.7983	-0.3017	1.4291	15.0	12.1738	-2.8262
1.3479	4.9	5.4331	0.5331	1.3922	8.1	9.1093	1.0093	1.4287	16.0	12.1359	-3.8641
1.3136	4.9	2.5861	-2.3139	1.3298	8.2	3.9302	-4.2698	1.4313	16.5	12.3569	-4.1431
1.3012	5.3	1.5587	-3.7413	1.4025	8.2	9.9618	1.7618				

Analysis of the depth values derived for the test subset (Table 1) reveals that for charted depths below 13 metres there are major discrepancies which accord with other research results so these soundings were excluded. The other chart soundings that show absolute differences of about 2.5metres are also highlighted in the table. When the position of these soundings were located on the chart, each was observed to be on part of the delta that would be subject to most short-term movement (on swash bar ridges or at points of steep drop in depth where minor errors in charting can cause a large discrepancy in depth value). It was therefore decided to remove these values from the calculation of RMSE value for the data set. The resultant RMSE value for depths to 13m was found to be 1.1566m which also compares favourably with the results documented in the Dekker et al. (2011) comparative study – RMSE values between between 0.85 and 2.3 m for semi-analytic methods and 1.68m for empirical derivation.

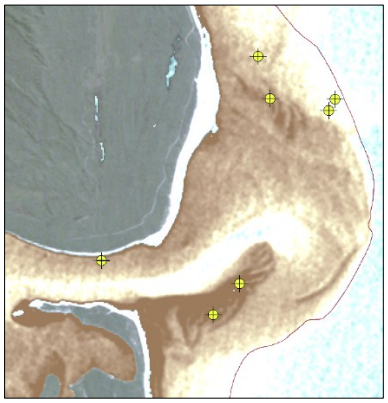

Figure 10: Yellow graphs mark the position of derived depths with absolute error greater than 2.5m. All were excluded from RMSE calculation

The accuracy to 13m and the RMSE value 1.1566m, which is an error margin of approximately 9% in waters to this depth, compares favourably to other research. In the Dekker et al. (2011) survey of optical depth retrieval algorithms, 13m was identified as the general limit of reliability for empirically based algorithms. Stumpf et al. (2003) argued the log transform algorithm was effective for depth to 15m, Lyzenga et al. (2006) documented reliable depth retrieval to approximately 15m, Brando et al. (2009) retrieved reliably correlated depths between 4 and 13m.

5.2 Image Analysis

5.2.1 Derived depth surfaces

The derived depth surfaces for each year are included in Appendix 3. The 20 equal interval classification was converted to a unique values which then identified the 0 return in the range. These 21 values were then calibrated to the calibrated 0.5m depth values. The utility of these images in identifying benthic morphology is illustrated in Figure 10 which juxtaposes images from 1987, 1994, 2001 and 2008. Each image shows a different configuration of the delta complex ranging from extensive growth of the southern spit, swash bar formation and movement across swash platform to bar welding on the down-drift shoreline.

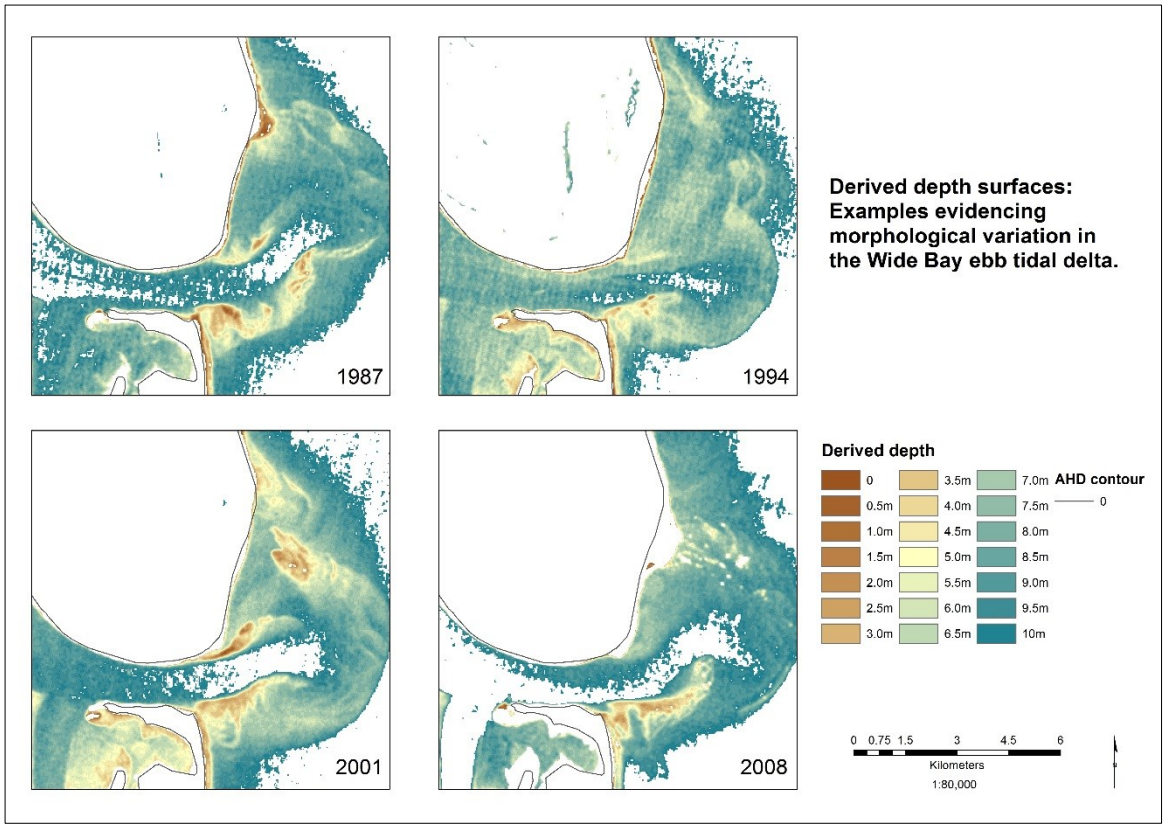

Figure 11: Derived depth surfaces- metre measurement derived from an equal interval classification of pixel values corrected to LAT 10m contour

An issue to note when 'reading' the images is that if part of the delta becomes sub-aerial – i.e. above the water line - a no data return results in a blank pixel value, for example the extensive white area of the northern spit in image 2008 representing bar welding to the shore line. Similarly if the pixel value fell below the defined depth of extinction (i.e. 10 metres) a no data value results in a colourless pixel, such as the areas within the main channel.

5.2.2 Difference images

Difference images based on the map algebra calculation of pixel value difference between consecutive years help identify regions of the delta undergoing the greatest change over the individual 12 month intervals. Figure 11 demonstrates the utility of these images because although change can be observed in the inset depth images, the Difference images highlight the magnitude of change between years. Pinpointing the location of maximum variation is an aid to inferring the shifting location of maximum flows and forcing currents acting on the delta.

Analysis of the difference images in Figure 11 suggests that the extreme deflection of the main channel evident in the depth image of 1987 had reached the point of unsustainable hydraulic inefficiency as between 1987 and 1988 the southern spit began to decompose. Investigating the difference image shows that maximum sediment loss occurred where strong ebb-tidal currents would be forcing sediment off the spit out towards the terminal lobe in increasingly extensive spillover channels. Once this pathway is established in the ensuing years the sediment is shifted out towards the terminal lobe in arcurate bars reflecting the directional forcing of the ebb current. Because of the existence of these bars longshore sediment transport is still bypassing the inlet evidenced by the increase in sediment north of the northern spit.

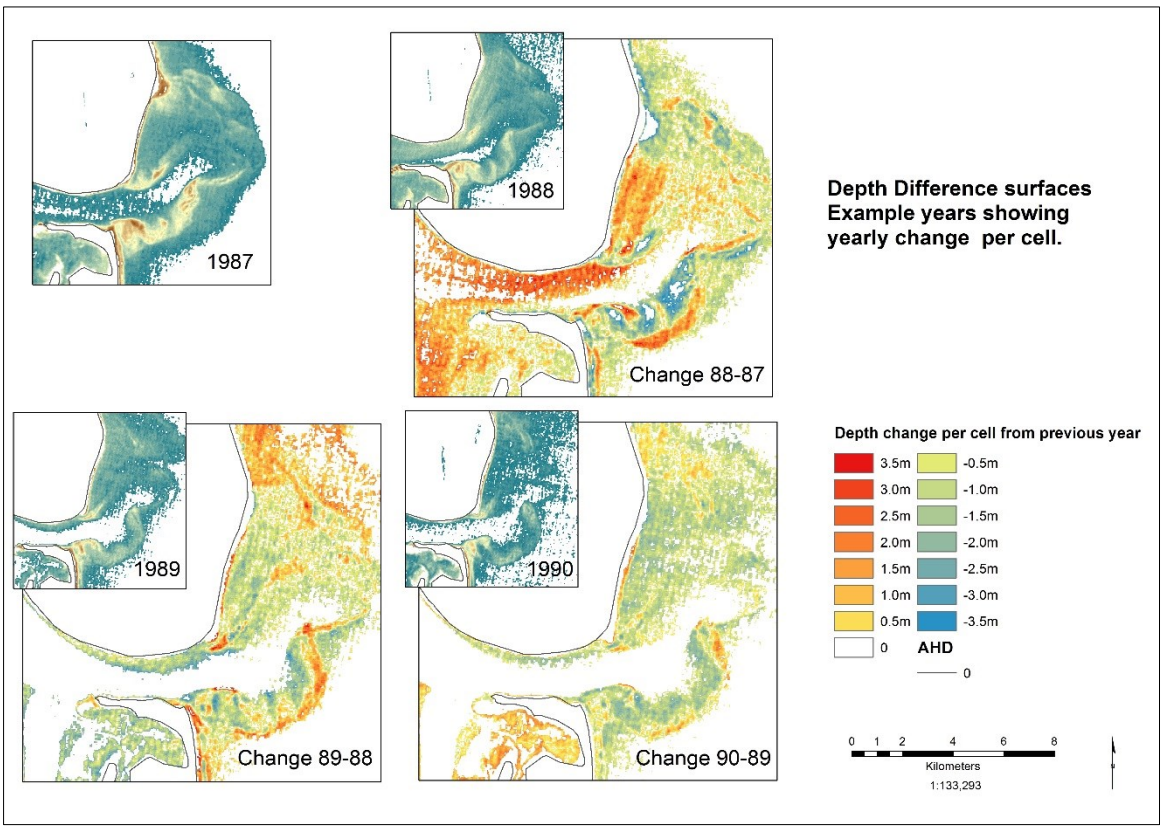

Figure 12: Difference surfaces for 1988-1990. Note that while the depth images show depth change, the difference surfaces emphasise the range of change

5.2.3 Variability of delta volume

The main data set evident in the previous images was further subset to include only the portion of the delta seaward of the inlet. The difference images were then interrogated to

investigate the volumetric changes evident in the depth variations. No benchmark volumes could be calculated but the variation of volume between years could be calculated on the basis of the sum of the product of each depth change value and pixel count and area. Area could be calculated as the product of pixel count and pixel area which in the case of Landsat images is $900m^2$- ie cell size is 30 x30m.

The ebb-tidal delta subset was further divided into northern and southern section sectioned along the mid line of the main ebb channel. The results of this calculation are shown in Figure 12 without increment as the focus of this analysis was variability not an absolute amount calculation.

It can be observed the area of the ebb delta as extant above the 10m depth contour is relatively consistent over the entire period of observation. However volumetric fluctuations are more pronounced. As well the graphs show grouped periods of volatility between 1988 and 1993 and 1998 and 2003 and the onset of volatility at 2008. This suggests that there is an 11 year cycle in the ebb-tidal delta behaviour, alternating between 6 years of volatility and 5 years of stability. The robustness of this observation need to be explored against concurrent observed variations in forcing agents.

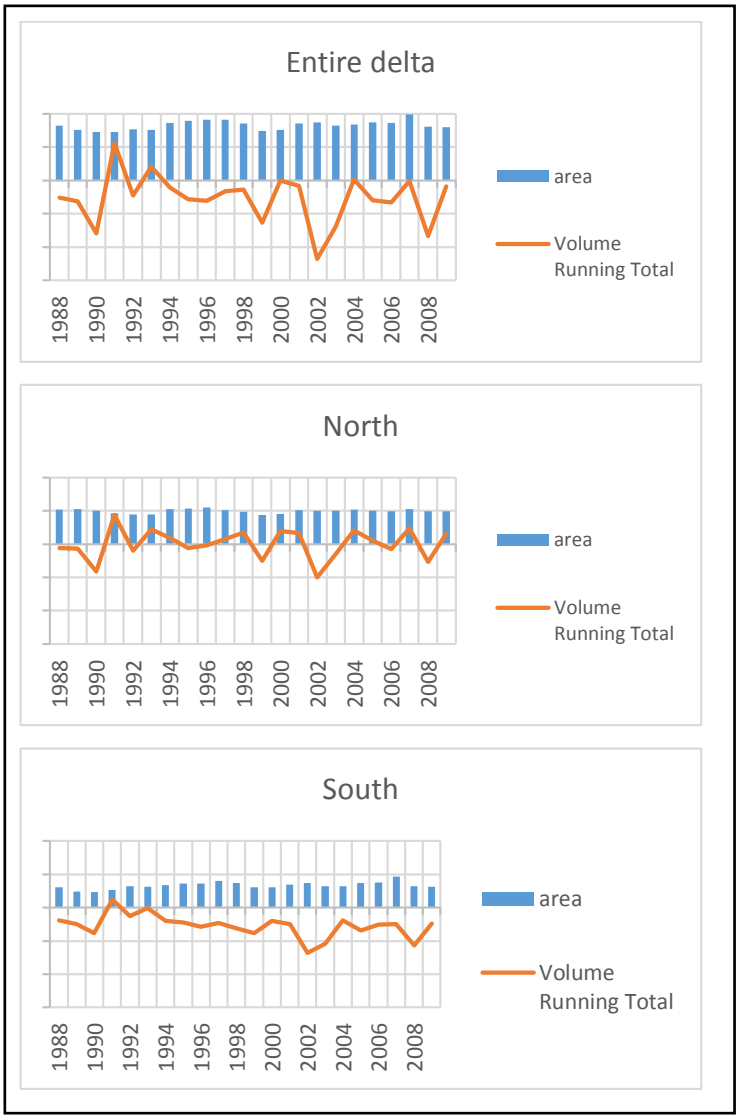

Figure 13: Spatial extent and volumetric variation of Wide Bay ebb-tidal delta calculated from derived difference surfaces. Units excluded base volume for delta unable to be derived so volumetric fluctuation scaled on change between years

5.2.4 Statistical surfaces

Following the methodology proposed by Mitasova et al. (2010), minimum, maximum, mean, majority and range depth surfaces were generated using cell statistics for the entire multiyear data set (Figure 13). The maximum value represented the deepest value of a particular pixel over the 26 year set so is the 'core' surface below which sediment on the delta is stationary. The minimum depth value is the 'envelope' below which sediment movement occurs. The majority surface represents the depth below which sediment movement is less likely and the range surface identifies areas of greater or lesser variability.

The minimum surface image reveals the spatial extent of significant bar and spit formation and the semi-stationary position of major spill-over channels and marginal flood channels. The maximum surface emphasises that most of the ebb tide delta is subject to significant sediment gain and loss but when read in concert with the mean surface, the usual existence of an up-drift terminal lobe and down drift swash platform confirm the ebb-tidal delta extent as an important element in sand bypassing the delta. The range image pinpoint maximum variation and informed the placement of transects to generate profile from these sets.

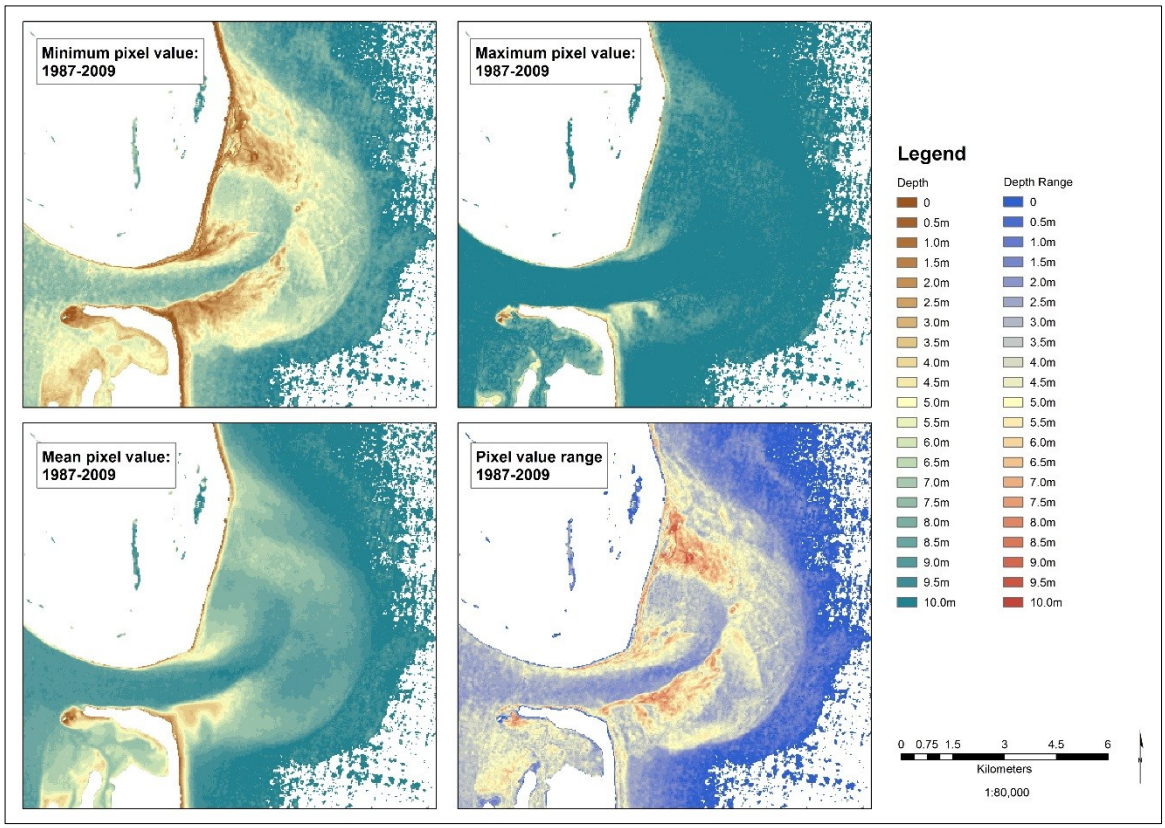

Figure 14: Statistical Minimum, maximum, mean and range surfaces derived from the application of cell statistics to the entire dataset. Method as described by (Mitasova et al., 2009)

5.2.5 Statistical surface profiles

Profiles were generated for minimum, mean and majority surfaces along transects drawn along regions of greatest depth variation as evident in the range surface: along the south spit, across the down drift swash platform, along the main channel and over the terminal lobe crest and across the main channel including the down-drift channel margin/attached bar system (Figure 14).

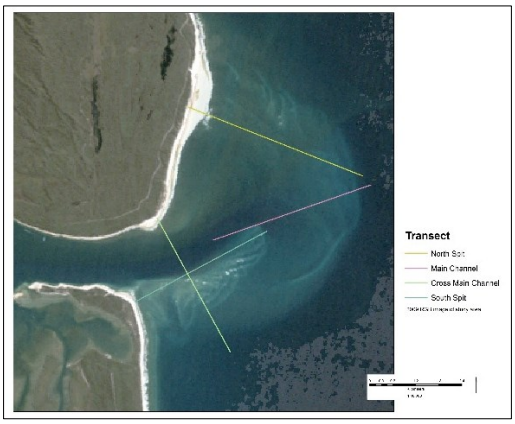

Figure 15: Transect locations used to generate statistical surface profile plots

Each of these profiles sets enable a number of spatial relationships to be explored and refine the regions of the delta most impacted by forcing agents.

5.2.5.1 The Southern Spit Transect

The transect plot (Figure 15) reveals that for the 1500 metres of the spit the depth is relatively stable but with variation in ridge placement. Beyond 1500m the existence of variation in the majority surface points to the development of spill over channels and hydraulic inefficiency becomes more pronounced when the spit has elongated and perturbed the main channel to the downdrift shoreline. The minimum extent of the spit along this transect appears to be 1200m with the existence of a marginal flood channel close to the shoreline, a common feature in both minimum and maximum surfaces. The variation in length may also infer quite substantial changes in longshore transport rates which need to be investigated against wave climate records for the delta.

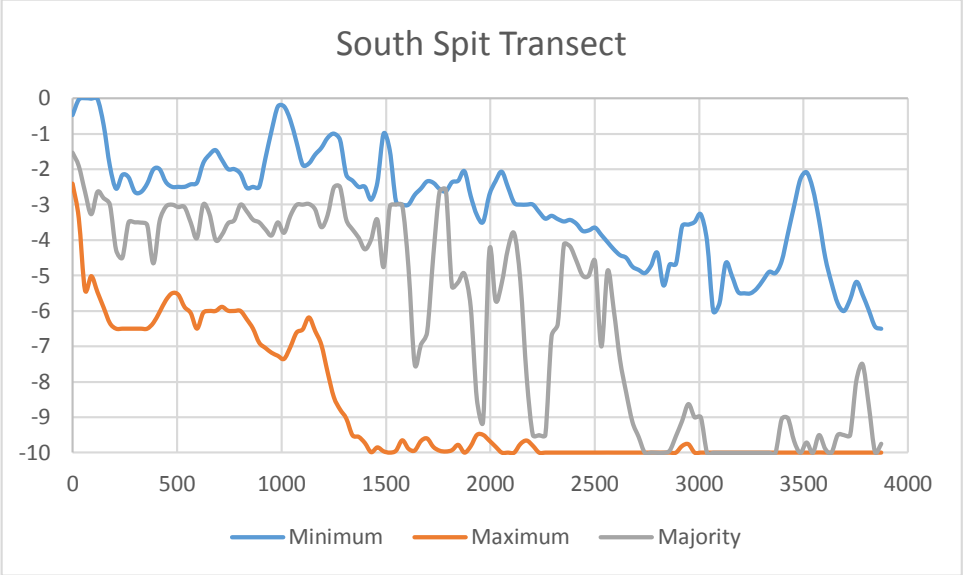

Figure 16: South Spit Transect plot: minimum, maximum and majority statistical surfaces

5.2.5.2 The North Spit/Swash Platform Transect

This transect runs from the area south of the easterly most landward point of ebb-tidal delta shoreline. This is an important consideration as bar welding to shoreline at this point is dependent on a decrease in LST currents. The statistical surfaces for this transect (Figure 16) show that onshore migration of swash bars at this point is much less frequent as evident in the majority surface being much more inclined to the maximum (core) rather than the minimum (envelop) depth surface Less sediment in this part of the swash platform implies sediment bypassing of the delta under the influence of longshore currents and as this is the majority situation it can be inferred that for the period of this study longshore currents exerted a considerable control on delta morphology.

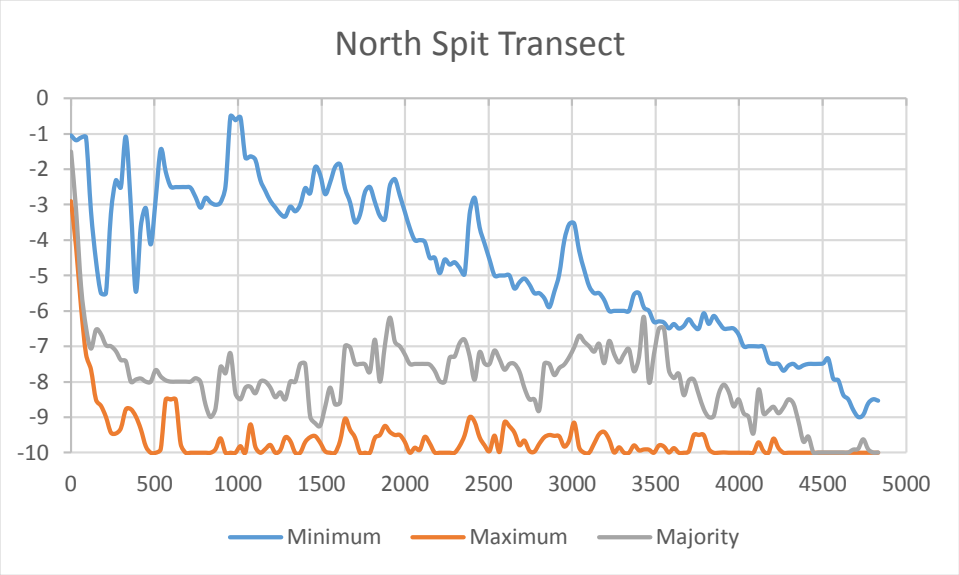

Figure 17: North Spit Transect: minimum, maximum and majority statistical surfaces

5.2.5.3 The Main Channel Transect

The main channel transect (Figure 17) provides evidence that the terminal lobe crest generally occurs at approximately the 2750m mark along the transect at a depth of between 7 and 8 metres. The minimum depth transect evidences the growth of the south spit when the channel is deflected to the down drift coast.

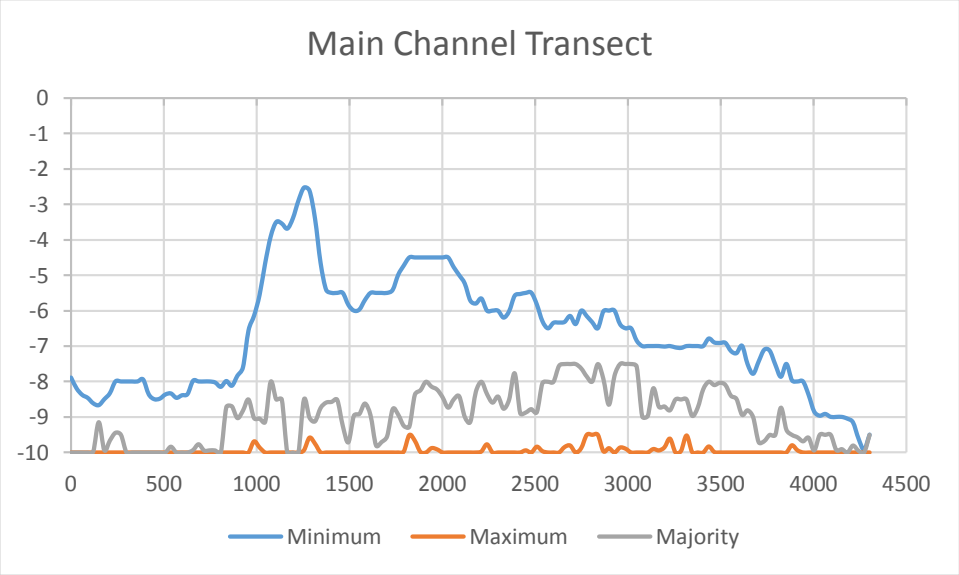

Figure 18: Main Channel Transect: minimum, maximum and majority statistical surfaces

5.2.5.4 Main Channel Cross section Transect

This transect taken near the seaward inlet opening displays the stability of the main channel and the variability of the channel linear bars and spits (Figure 18). The up-drift section (0-

1000m) displays the irregularity of extensive marginal channel bars as the minimum surface is distant from the majority surface at this point. Each surface does reveal the stability of a marginal flood channel between the bar maximum and the shoreline welding point. This is a very stable feature between the shoreline and approximately 300m along the transect. The up-drift channel margin bar (1500-2000m) is incorporated into the southern spit complex and the size of the dynamic layer between minimum and majority surface indicates the fluctuation of longshore sediment trapped in or bypassing the ebb-tidal delta complex.

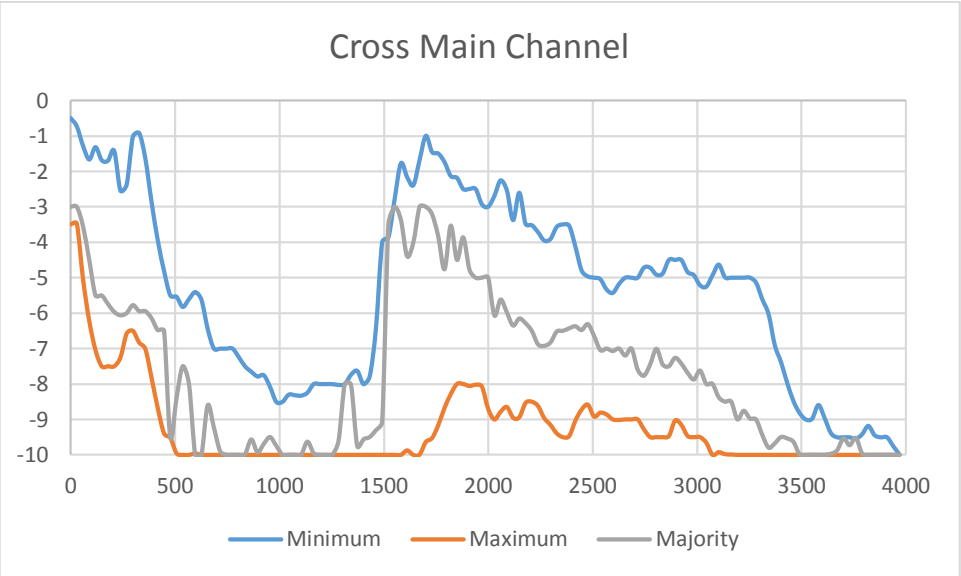

Figure 19: Cross Main Channel: minimum, maximum and majority statistical surfaces

6 Discussion

The objective of this research was to investigate the utility of Landsat satellite imagery for identifying ebb-tidal delta morphology through the derivation of bathymetric surfaces by implementing the shallow water depth retrieval Ratio Transform algorithm developed by Stumpf et al. (2003). The results of the validation processes as outlined previously, compared favourably to the results of other researchers and inspired confidence in using the derived depth layers to conduct spatial and statistical analysis of the 23 year time series data set. This analysis was able to confirm that key morphological elements of the ebb-tidal delta were clearly identifiable as was the variation in the morphology of the delta over time. The 23 year span of the data set enabled analysis of cyclic fluctuations of the delta and comparison with other time series studies. Finally observed fluctuations could be compared to fluctuations in the SOI and IPO to investigate potential climate forcing mechanisms acting on the Wide Bay ebb-tidal delta.

6.1 Morphological elements.

The derived depth surfaces clearly display the prototypical morphodynamics of an ebb-tidal delta as described in FitzGerald and Miner (2013), Hayes and FitzGerald (2013) and Hayes (1980). In addition it conforms to patterns identified in FitzGerald et al. (2000b), Kana et al. (1999) and Kraus (2005) for inlets subject to significant longshore forcing: periodic growth and perturbation of the up-drift channel margin spit with sediment bypassing the inlet along the terminal lobe, followed by breaching events and sediment transfer to the down drift swash platform and subsequent migration of swash bars across the platform to ultimately weld on the down-drift shoreline. Marginal flood channels are clearly evident as are lateral movements of spill-over channels. Movement of shore welded bars along the up-drift shoreline concurs with wave generated current forcing and reversals in longshore currents augmenting flood currents along down-drift isolated beaches (Kraus, 2005), leading to shoreline erosion and increased sediment re-entering the inlet. Figure 19 illustrates the level of detail able to be extracted from the dataset with effective visualisation of morphological change between time slices.

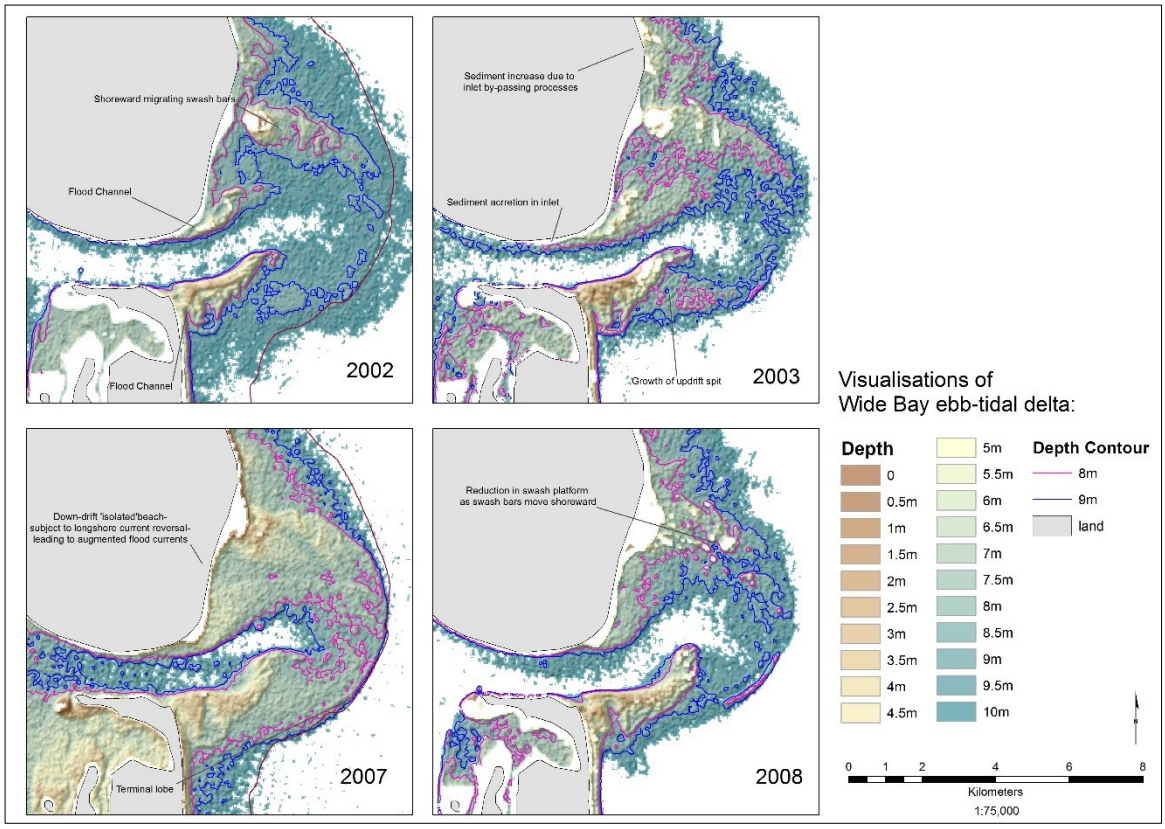

Figure 20: Visualisation of ebb-tidal delta. Relative depth surface overlaid on hillshade surfaces. 2002/2003 panels evidence swash platform and terminal lobe accreting. 2007/2008 show swash platform deflating.

In Figure 19 it can be observed that the 2002/2003 images suggest sediment moving from the back barrier through the inlet to accrete on the channel margins leading to extension of both the up and down-drift bar complexes as well as increasing the volume of the down-drift swash platform. Conversely the 2007/2008 images display the opposite tendency. The back barrier has gained sediment as evident in the 'no data' blank area along the inner edge of the recurved spit in the 2008 image. In addition there has been a deflation of the down drift portion of the terminal lobe and a net landward movement of sediment across the swash platform and significant bar welding along the down-drift coast.

These dynamics, comprehensively discussed in conceptual models such the FitzGerald et al. (2000a) suite, have also been observed in numerous empirical studies of ebb- tidal behaviour (Fitzgerald and Nummedal, 1983, Ruggiero et al., 2005, Gaudiano and Kana, 2001, Sha, 1989, Vinther et al., 2004, Costas and FitzGerald, 2011). Such studies had typically utilised historical photography, survey records or more recently LiDAR imagery to document change, with the

inherent limitation of these studies being the intervals between records and the inability to fully document subtle changes in the morphodynamic cascade.

6.2 Process analysis

The capacity to build a contiguous record of morphological change from satellite imagery, with spatial resolution to identify incremental changes in morphological units presents an opportunity to investigate the interaction of tide and wave forcings on the delta as these are the fundamental processes shaping ebb-tidal delta morphology and proximate shorelines (Kana et al., 1999, Kraus and Kim, 2009). This research project's contour maps of the Wide Bay derived depth data clearly demonstrate the level of inter-annual and inter-decadal morphological variability able to be detected from the satellite imagery. Figure 20 contains the entire time series, imaged as 5, 8 and 9 metre contours. This combination best visualises the shifts in location of the main ebb channel, terminal lobe and spit elongation and bar welding events.

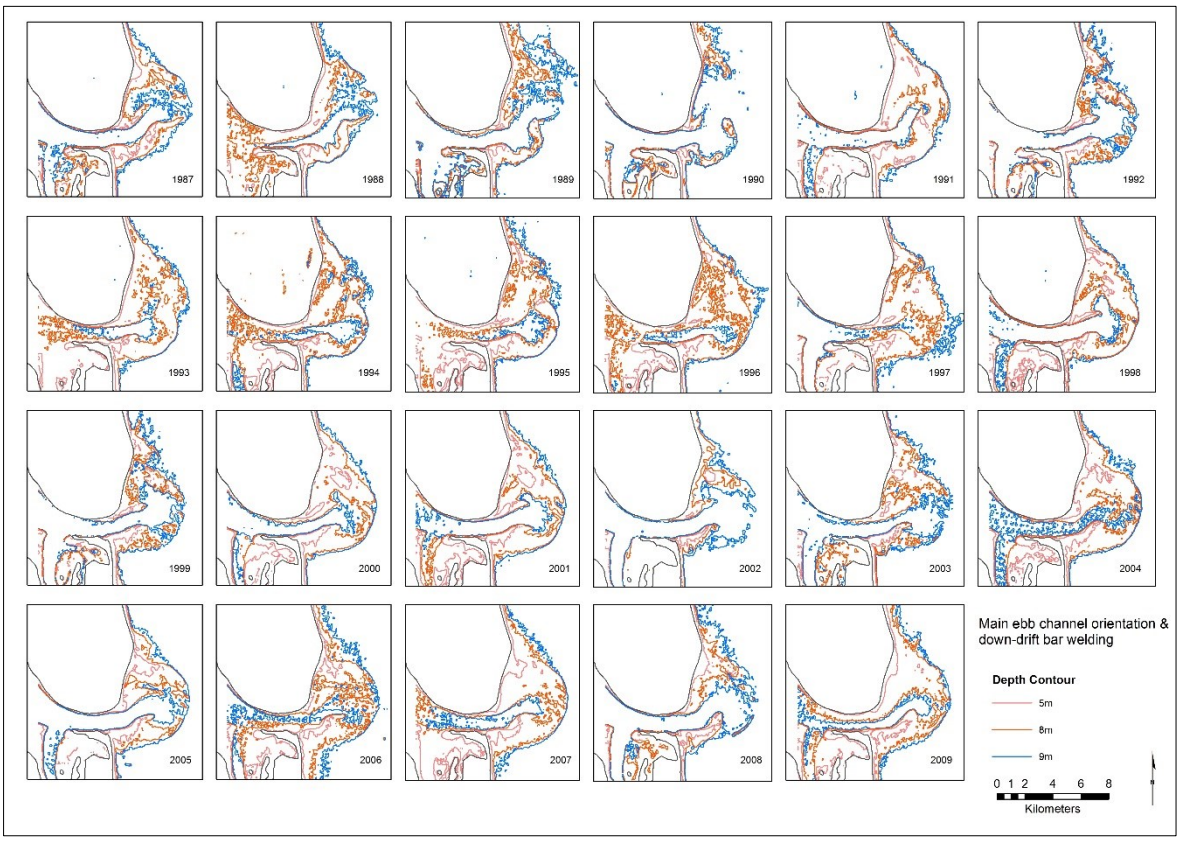

Figure 21: Entire Time Series of Wide Bay ebb-tidal delta visualised at 5, 8 and 9 metre contours.

It is immediately evident that the orientation of the main channel rotates through approximately a sixty degree angle from the north-east to the east south-east. This rotation is evident at the outer extent of the channel so that the ebb delta appears to conform the outer channel shifting model described by FitzGerald et al. (2000a). The NE orientation of the channel is the minority position for this time series as after 1992 the predominant orientation is easterly. It is also evident that there is a twelve year interval between instances of minimal delta volume (1990 and 2002).

The variability in the time series contour images reflects the volumetric variability evident in the calculation of difference volumes discussed earlier in this paper. The area and volumes for the entire delta evident in Figure 12, indicate a stable 'footprint' for the delta- i.e. area- as opposed to the variability in volume. Changes in volume on the delta appear from the graph to oscillate between years of relative stability punctuated by large fluctuations in delta volume. This finding is similar to that observed by Morgan et al. (2011) and cycles of barrier stability described by (Masselink and Van Heteren, 2014).

Wide Bay ebb-tidal delta in this research is observed to have 2 distinct periods of delta volumetric variability: between 1988 and 1993, and again between 1998 and 2003. There is then an emergent period of instability in the years 2007-2009.

During both periods of fluctuation there is maximum rotation of main channel orientation and significant reduction in the site of the teminal lobe at its spillover point, as well as major deflations of the swash platform. Both these morphological changes indicate changes in incident wave direction as well as shifting balances between wave current energy and tidal current energy. As previously reported the wave climate on this section of the Australian coast fluctuates between a uni-modal SE climate and a bi-modal E and SSE wave climate (Goodwin et al., 2013). These wave climates reflect oscillations in atmospheric climate indices particularly the Southern Oscillation Index (SOI) and the Interdecadal Pacific Oscillation (IPO). Accordingly, the periods of delta instability were compared to recorded SOI/IPO values for the study interval as illustrated in Figure 21.

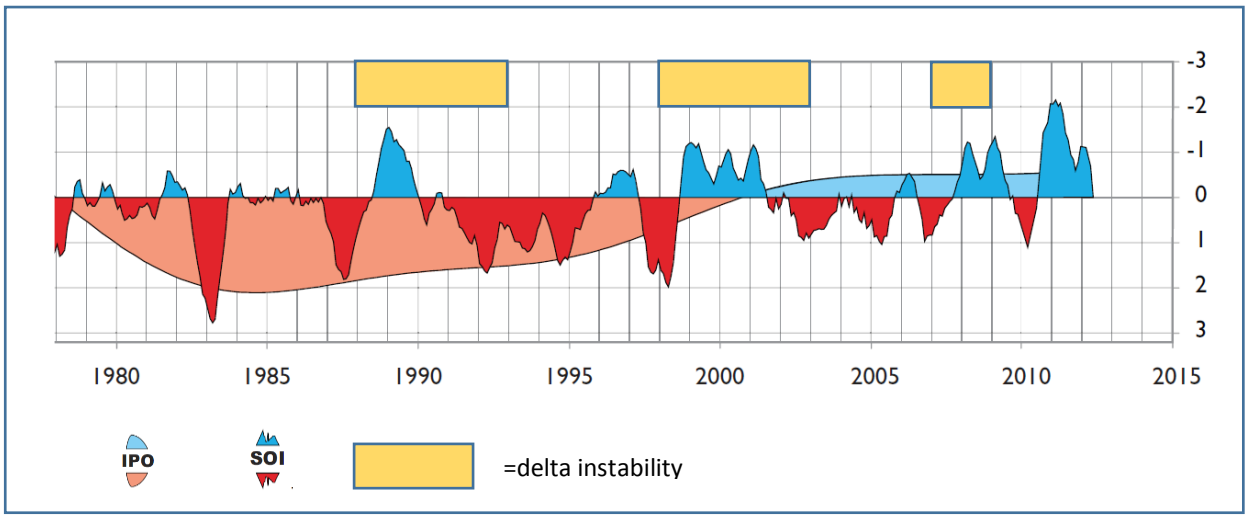

Figure 22: Periods of delta fluctuation correlated to SOI and IPO. Figure based on IPO SOI visualisation in Queensland Government publication- Australia's Variable Rainfall (DSITIA, 2014).

The correlation of delta instability with the onset of SOI La Nina events with an SOI value less than -1 confirms the dependency of delta behaviour on dominant climate forcing agents. In turn, understanding the morphological response of the ebb delta to these forcings can inform projection of shoreline behaviour adjacent to the delta. The ability to map these morphological manifestations then offers the possibility of developing shoreline morphological signatures of climate driven delta variation. Understanding the forcing agents responsible for such signatures, may provide insights into past climate events recorded in the paleo record.

6.3 Future research potential

The evidence of observable ebb-tidal delta periodicity in this derived data set, holds promise that detailed observations of nearshore behaviour in the optical satellite record can be linked to detailed observations of shoreline and back barrier behaviour to develop a comprehensive understanding of 'Coastal Tract' compartments (Cowell et al., 2003a). The work of Hansen et al. (2013) and Barnard et al. (2012) on down-drift coastline retreat due to changes, anthropogenic and natural, to the San Francisco Bay ebb-tidal delta highlight the impact of delta deflation on bar welding sequences and the effects of changes to shoreline exposure to wave energy. These studies synthesise a range of data sources including historical charts and contemporary LiDAR surveys, yet the record of the nearshore is still intermittent as compared to that of the terrestrial coast. As an 'unengineered' inlet, the Wide Bay inlet provides the opportunity to investigate responses to natural forcings as evident in the instrumental and sedimentary record. Detailed empirical study for the period of the Landsat archival record can

contribute to more a nuanced understanding of nearshore variability than has previously been available to coastal geomorphologists.

The particular method used in this study may prove to be limited in application to waters with low turbidity and with predominantly sandy substrate, however this does not diminish the promise that the method holds for nearshore sites which satisfy those criteria.

7 Conclusion

Comprehensive investigation of the nearshore compartment has confounded coastal geomorphologists due to the difficulty in obtaining bathymetric data (Ruggiero et al., 2005). On sedimentary coasts which exhibit high levels of geomorphic dynamism, the length of time between survey data has meant that studies of coastline response to forcing mechanisms have relied on extensive interpolation from existing data or resorted to modelled behaviour based on engineering generalisation (for example the Bruun Rule). The application of depth retrieval using the optical satellite record affords coastal geomorphologists with a four decade long archive of nearshore morphological behaviour.

This research has shown that the Landsat archive and the IHO methodology can be used to derive time series bathymetric surfaces which detail morphological dynamism hitherto undocumented due to technological limitations or prohibitive costs associated with available survey methods. The time series data generated evidenced cyclical behaviour in ebb-tidal delta morphology which could be correlated to shifts in climatic forcing events such as shifts in the ENSO index and the IPO. This data enables a robust analysis of the interaction of natural forcings, sediment movement in the near shore and the impact on the adjacent shoreline position.

While preliminary in its conclusions, this research report highlights the potential of the method to expand the coastal geomorphologist community's understanding of what is really happening in the sub-aqueous nearshore environment.

8 References

2014. 2014 Queensland Tide Tables Standard Port Tide Times. *In:* QUEENSLAND, D. O. T. A. M. R. (ed.). Brisbane.

ASHTON, A. D. & MURRAY, A. B. 2006. High-angle wave instability and emergent shoreline shapes: 2. Wave climate analysis and comparisons to nature. *Journal of Geophysical Research: Earth Surface,* 111**,** F04012.

BARNARD, P. L., HANSEN, J. E. & ERIKSON, L. H. 2012. Synthesis Study of an Erosion Hot Spot, Ocean Beach, California. *Journal of Coastal Research,* 28**,** 903-922.

BECK, T. M. & KRAUS, N. C. 2011. New Ebb-Tidal Delta at an Old Inlet, Shark River Inlet, New Jersey. *Journal of Coastal Research***,** 98-110.

BERTIN, X., FORTUNATO, A. B. & OLIVEIRA, A. 2009. A modeling-based analysis of processes driving wave-dominated inlets. *Continental Shelf Research,* 29**,** 819-834.

BIERWIRTH, P., LEE, T. & BURNE, R. 1993. Shallow sea-floor reflectance and water depth derived by unmixing multispectral imagery. *Photogrammetric Engineering and Remote Sensing,* 59**,** 331-338.

BOYD, R., DALRYMPLE, R. & ZAITLIN, B. A. 1992. Classification of clastic coastal depositional environments. *Sedimentary Geology,* 80**,** 139-150.

BOYD, R., RUMING, K., GOODWIN, I., SANDSTROM, M. & SCHRÖDER-ADAMS, C. 2008. Highstand transport of coastal sand to the deep ocean: A case study from Fraser Island, southeast Australia. *Geology,* 36**,** 15-18.

BRANDO, V. E., ANSTEE, J. M., WETTLE, M., DEKKER, A. G., PHINN, S. R. & ROELFSEMA, C. 2009. A physics based retrieval and quality assessment of bathymetry from suboptimal hyperspectral data. *Remote Sensing of Environment,* 113**,** 755-770.

BRAYSHAW, S. & LEMCKERT, C. 2012. Pitfalls of Shoreline Stabilisation – Tweed River Mouth, Gold Coast, Australia. *In:* COOPER, J. A. G. & PILKEY, O. H. (eds.) *Pitfalls of Shoreline Stabilization.* Springer Netherlands.

BURNS, B., TAYLOR, J. & SIDHU, H. 2010. Uncertainties in bathymetric retrievals. *IOP Conference Series: Earth and Environmental Science,* 11**,** 012032.

CAPO, S., MARIEU, V., BRU, D., LUBAC, B. & BONNETON, P. 2013. Decadal morphodynamics evolution of a mixed-energy inlet using multispectral SPOT imagery. *Coastal Dynamics 2013*.

CASTELLE, B., BOURGET, J., MOLNAR, N., STRAUSS, D., DESCHAMPS, S. & TOMLINSON, R. 2007. Dynamics of a wave-dominated tidal inlet and influence on adjacent beaches, Currumbin Creek, Gold Coast, Australia. *Coastal Engineering,* 54**,** 77-90.

COLLIN, A. & HENCH, J. L. 2012. Towards Deeper Measurements of Tropical Reefscape Structure Using the WorldView-2 Spaceborne Sensor. *Remote Sensing,* 4**,** 1425-1447.

COOPER, J. A. G., MCKENNA, J., JACKSON, D. & O'CONNOR, M. 2007. Mesoscale coastal behavior related to morphological self-adjustment. *Geology,* 35**,** 187-190.

COSTAS, S. & FITZGERALD, D. 2011. Sedimentary architecture of a spit-end (Salisbury Beach, Massachusetts): The imprints of sea-level rise and inlet dynamics. *Marine Geology,* 284**,** 203-216.

COWELL, P. J., STIVE, M. J. F., NIEDORODA, A. W., DE VRIEND, H. J., SWIFT, D. J. P., KAMINSKY, G. M. & CAPOBIANCO, M. 2003a. The Coastal-Tract (Part 1): A Conceptual Approach to Aggregated Modeling of Low-Order Coastal Change. *Journal of Coastal Research,* 19**,** 812-827.

COWELL, P. J., STIVE, M. J. F., NIEDORODA, A. W., SWIFT, D. J. P., DE VRIEND, H. J., BUIJSMAN, M. C., NICHOLLS, R. J., ROY, P. S., KAMINSKY, G. M., CLEVERINGA, J., REED, C. W. & DE BOER, P. L. 2003b. The Coastal-Tract (Part

2): Applications of Aggregated Modeling of Lower-order Coastal Change. *Journal of Coastal Research,* 19**,** 828-848.

DAVIDSON-ARNOTT, R. 2011. 3.04 - Wave-Dominated Coasts. *In:* EDITORS-IN-CHIEF: ERIC, W. & DONALD, M. (eds.) *Treatise on Estuarine and Coastal Science.* Waltham: Academic Press.

DAWSON, R. J., DICKSON, M. E., NICHOLLS, R. J., HALL, J. W., WALKDEN, M. J. A., STANSBY, P. K., MOKRECH, M., RICHARDS, J., ZHOU, J., MILLIGAN, J., JORDAN, A., PEARSON, S., REES, J., BATES, P. D., KOUKOULAS, S. & WATKINSON, A. R. 2009. Integrated analysis of risks of coastal flooding and cliff erosion under scenarios of long term change. *Climatic Change,* 95**,** 249-288.

DEKKER, A. G., PHINN, S. R., ANSTEE, J., BISSETT, P., BRANDO, V. E., CASEY, B., FEARNS, P., HEDLEY, J., KLONOWSKI, W., LEE, Z. P., LYNCH, M., LYONS, M., MOBLEY, C. & ROELFSEMA, C. 2011. Intercomparison of shallow water bathymetry, hydro-optics, and benthos mapping techniques in Australian and Caribbean coastal environments. *Limnology and Oceanography-Methods,* 9**,** 396-425.

DISSANAYAKE, D. M. P. K., ROELVINK, J. A. & VAN DER WEGEN, M. 2009. Modelled channel patterns in a schematized tidal inlet. *Coastal Engineering,* 56**,** 1069-1083.

DODET, G., BERTIN, X., BRUNEAU, N., FORTUNATO, A. B., NAHON, A. & ROLAND, A. 2013. Wave-current interactions in a wave-dominated tidal inlet. *Journal of Geophysical Research C: Oceans,* 118**,** 1587-1605.

DOXANI, G., PAPADOPOULOU, M., LAFAZANI, P., PIKRIDIS, C. & TSAKIRI-STRATI, M. 2012. Shallow-water bathymetry over variable bottom types using Multispectral Worldview-2 image. *XXII ISPRS Congres.* Melbourne, Australia: International Archives of the Photogrammetry, Remote Sensing and Spatial Information Sciences.

DSITIA. 2014. *Australia's Variable Rainfall* [Online]. Queensland Government. Available: https://www.longpaddock.qld.gov.au/products/australiasvariableclimate/ [Accessed 20/6/2015 2014].

DYER, K. R. & HUNTLEY, D. A. 1999. The origin, classification and modelling of sand banks and ridges. *Continental Shelf Research,* 19**,** 1285-1330.

FITZGERALD, D. M., FENSTER, M. S., ARGOW, B. A. & BUYNEVICH, I. V. 2008. Coastal Impacts Due to Sea-Level Rise. *Annual Review of Earth and Planetary Sciences,* 36**,** 601-647.

FITZGERALD, D. M., KRAUS, N. C. & HANDS, E. B. 2000a. *Natural mechanisms of sediment bypassing at tidal inlets*, US Army Corps of Engineers Vicksburg, MS.

FITZGERALD, D. M., KRAUS, N. C. & HANDS, E. B. 2000b. Natural Mechanisms of sediment bypassing at Tidal Inlets. *Coastal and Hydraulics Engineering Technical Note,* IV.

FITZGERALD, D. M. & MINER, M. D. 2013. Tidal inlets and lagoons along siliciclastic barrier coasts. *In:* SHRODER, J. (ed.) *Treatise on Geomorphology.* San Diego CA: Academic Press.

FITZGERALD, D. M. & NUMMEDAL, D. 1983. RESPONSE CHARACTERISTICS OF AN EBB-DOMINATED TIDAL INLET CHANNEL. *Journal of Sedimentary Petrology,* 53**,** 833-845.

FRENCH, J. R. & BURNINGHAM, H. 2013. Coasts and climate: Insights from geomorphology. *Progress in Physical Geography,* 37**,** 550-561.

GAO, J. 2009. Bathymetric mapping by means of remote sensing: methods, accuracy and limitations. *Progress in Physical Geography,* 33**,** 103-116.

GAUDIANO, D. J. & KANA, T. W. 2001. Shoal Bypassing in Mixed Energy Inlets: Geomorphic Variables and Empirical Predictions for Nine South Carolina Inlets. *Journal of Coastal Research,* 17**,** 280-291.

GOODWIN, I. 2014. *RE: Vorticity in flood channels.* Type to BURKE, A.

GOODWIN, I. D. 2005. A mid-shelf, mean wave direction climatology for southeastern Australia, and its relationship to the El Nino-Southern Oscillation since 1878 AD. *International Journal of Climatology,* 25**,** 1715-1729.

GOODWIN, I. D., FREEMAN, R. & BLACKMORE, K. 2013. An insight into headland sand bypassing and wave climate variability from shoreface bathymetric change at Byron Bay, New South Wales, Australia. *Marine Geology,* 341**,** 29-45.

HANSEN, J. E., ELIAS, E. & BARNARD, P. L. 2013. Changes in surfzone morphodynamics driven by multi-decadal contraction of a large ebb-tidal delta. *Marine Geology*.

HARLEY, M. D., TURNER, I. L., SHORT, A. D. & RANASINGHE, R. 2011. A reevaluation of coastal embayment rotation: The dominance of cross-shore versus alongshore sediment transport processes, Collaroy-Narrabeen Beach, southeast Australia. *Journal of Geophysical Research F: Earth Surface,* 116.

HAYES, M. O. 1980. General morpology and sediment patterns in tidal inlets. *Sedimentary Geology***,** 139-156.

HAYES, M. O. & FITZGERALD, D. M. 2013. Origin, Evolution, and Classification of Tidal Inlets. *Journal of Coastal Research***,** 14-33.

HEDLEY, J. D., HARBORNE, A. R. & MUMBY, P. J. 2005. Technical note: Simple and robust removal of sun glint for mapping shallow-water benthos. *International Journal of Remote Sensing,* 26**,** 2107-2112.

HENNECKE, W. G. & COWELL, P. I. 2000. GIS modeling of impacts of an accelerated rate of sea-level rise on coastal inlets and deeply embayed shorelines. *Environmental Geosciences,* 7**,** 137-148.

HU, C. M. 2008. Ocean color reveals, sand ridge morphology on the west Florida shelf. *Ieee Geoscience and Remote Sensing Letters,* 5**,** 443-447.

IHO 2013. *The IHO-IOC GEBCO Cook Book*.

KANA, T. W., HAYTER, E. J. & WORK, P. A. 1999. Mesoscale sediment transport at southeastern US tidal inlets: Conceptual model applicable to mixed energy settings. *Journal of Coastal Research,* 15**,** 303-313.

KANA, T. W., ROSATI, J. D. & TRAYNUM, S. B. 2011. Lack of Evidence for Onshore Sediment Transport from Deep Water at Decadal Time Scales: Fire Island, New York. *Journal of Coastal Research***,** 61-75.

KANNO, A., TANAKA, Y., KUROSAWA, A. & SEKINE, M. 2013. Generalized Lyzenga's Predictor of Shallow Water Depth for Multispectral Satellite Imagery. *Marine Geodesy,* 36**,** 365-376.

KRAUS, N. C. 2005. *Coastal inlet functional design: Anticipating morphologic response*, Defense Technical Information Center.

KRAUS, N. C. & KIM, Y. 2009. Engineering of tidal inlets and morphologic consequences. Chapter.

LEE, K. R., OLSEN, R. C. & KRUSE, F. A. 2012. Using multi-angle WorldView-2 imagery to determine ocean depth near the island of Oahu, Hawaii. *In:* SHEN, S. S. & LEWIS, P. E. (eds.) *Algorithms and Technologies for Multispectral, Hyperspectral, and Ultraspectral Imagery Xviii.*

LEE, Z., CARDER, K. L., MOBLEY, C. D., STEWARD, R. G. & PATCH, J. S. 1999. Hyperspectral remote sensing for shallow waters. 2. Deriving bottom depths and water properties by optimization. *Applied Optics,* 38**,** 3831-3843.

LEE, Z., CASEY, B., ARNONE, R., WEIDEMANN, A., PARSONS, R., MONTES, M. J., GAO, B. C., GOODE, W., DAVIS, C. O. & DYE, J. 2007. Water and bottom properties of a coastal environment derived from Hyperion data measured from the EO-1 spacecraft platform. *Journal of Applied Remote Sensing,* 1.

LEON, J. X., PHINN, S. R., HAMYLTON, S. & SAUNDERS, M. I. 2013. Filling the 'white ribbon' - a multisource seamless digital elevation model for Lizard Island, northern Great Barrier Reef. *International Journal of Remote Sensing,* 34**,** 6337-6354.

LIRIA, P., GAREL, E. & URIARTE, A. 2009. The effects of dredging operations on the hydrodynamics of an ebb tidal delta: Oka Estuary, northern Spain. *Continental Shelf Research,* 29**,** 1983-1994.

LYZENGA, D. R. 1978. Passive remote sensing techniques for mapping water depth and bottom features. *Applied Optics,* 17**,** 379-383.

LYZENGA, D. R., MALINAS, N. P. & TANIS, F. J. 2006. Multispectral bathymetry using a simple physically based algorithm. *Geoscience and Remote Sensing, IEEE Transactions on,* 44**,** 2251-2259.

MA, S., TAO, Z., YANG, X. F., YU, Y., ZHOU, X. & LI, Z. W. 2014. Bathymetry Retrieval from Hyperspectral Remote Sensing Data in Optical-Shallow Water. *Ieee Transactions on Geoscience and Remote Sensing,* 52**,** 1205-1212.

MARITORENA, S., MOREL, A. & GENTILI, B. 1994. DIFFUSE-REFLECTANCE OF OCEANIC SHALLOW WATERS - INFLUENCE OF WATER DEPTH AND BOTTOM ALBEDO. *Limnology and Oceanography,* 39**,** 1689-1703.

MASSELINK, G. & VAN HETEREN, S. 2014. Response of wave-dominated and mixed-energy barriers to storms. *Marine Geology,* 352**,** 321-347.

MATHER, P. M. & KOCH, M. 2011. *Computer processing of remotely-sensed images: an introduction,* Chichester, Wiley-Blackwell.

MITASOVA, H., HARDIN, E., OVERTON, M. F. & KURUM, M. O. 2010. Geospatial analysis of vulnerable beach-foredune systems from decadal time series of lidar data. *Journal of Coastal Conservation,* 14**,** 161-172.

MITASOVA, H., OVERTON, M. F., RECALDE, J. J., BERNSTEIN, D. J. & FREEMAN, C. W. 2009. Raster-Based Analysis of Coastal Terrain Dynamics from Multitemporal Lidar Data. *Journal of Coastal Research***,** 507-514.

MORGAN, K. M., KENCH, P. S. & FORD, R. B. 2011. Geomorphic change of an ebb-tidal delta: Mair Bank, Whangarei Harbour, New Zealand. *New Zealand Journal of Marine and Freshwater Research,* 45**,** 15-28.

MSQ. 2009. *Great Sandy Strait- South*.

O'CONNOR, M. C., COOPER, J. A. G. & JACKSON, D. W. T. 2011. Decadal behavior of tidal inlet-associated beach systems, northwest ireland, in relation to climate forcing. *Journal of Sedimentary Research,* 81**,** 38-51.

PE'ERI, S., PARRISH, C., AZUIKE, C., ALEXANDER, L. & ARMSTRONG, A. 2014. Satellite Remote Sensing as a Reconnaissance Tool for Assessing Nautical Chart Adequacy and Completeness. *Marine Geodesy,* 37**,** 293-314.

PERILLO, G. M. E. & PICCOLO, M. C. 2011. 1.02 - Global Variability in Estuaries and Coastal Settings. *In:* EDITORS-IN-CHIEF: ERIC, W. & DONALD, M. (eds.) *Treatise on Estuarine and Coastal Science.* Waltham: Academic Press.

PHILPOT, W. D. 1989. Bathymetric mapping with passive multispectral imagery. *Applied Optics,* 28**,** 1569-1578.

QUEENSLAND, S. O. 2013. Tidal Data. *In:* ROADS, D. O. T. A. M. (ed.).

ROY, P. S., WILLIAMS, R. J., JONES, A. R., YASSINI, I., GIBBS, P. J., COATES, B., WEST, R. J., SCANES, P. R., HUDSON, J. P. & NICHOL, S. 2001. Structure and function of south-east Australian estuaries. *Estuarine, Coastal and Shelf Science,* 53**,** 351-384.

RUGGIERO, P., KAMINSKY, G. A., GELFENBAUM, G. & VOIGT, B. 2005. Seasonal to interannual morphodynamics along a high-energy dissipative littoral cell. *Journal of Coastal Research,* 21**,** 553-578.

SANCHEZ-CARNERO, N., OJEDA-ZUJAR, J., RODRIGUEZ-PEREZ, D. & MARQUEZ-PEREZ, J. 2014. Assessment of different models for bathymetry calculation using SPOT multispectral images in a high-turbidity area: the mouth of the Guadiana Estuary. *International Journal of Remote Sensing,* 35**,** 493-514.

SEMINACK, C. T. & BUYNEVICH, I. V. 2013. Sedimentological and geophysical signatures of a relict tidal inlet complex along a wave-dominated barrier: Assateague Island, Maryland, U.S.A. *Journal of Sedimentary Research,* 83**,** 132-144.

SHA, L. P. 1989. Variation in ebb-delta morphologies along the West and East Frisian Islands, The Netherlands and Germany. *Marine Geology,* 89**,** 11-28.

SHERMAN, D. J. 2013. 10.1 Perspectives on Coastal Geomorphology: Introduction. *In:* SHRODER, J. F. (ed.) *Treatise on Geomorphology.* San Diego: Academic Press.

SHORT, A. D. & JACKSON, D. W. T. 2013. 10.5 Beach Morphodynamics. *In:* SHRODER, J. F. (ed.) *Treatise on Geomorphology.* San Diego: Academic Press.

SLOTT, J. M., MURRAY, A. B., ASHTON, A. D. & CROWLEY, T. J. 2006. Coastline responses to changing storm patterns. *Geophysical Research Letters,* 33.

SPLINTER, K. D., DAVIDSON, M. A., GOLSHANI, A. & TOMLINSON, R. 2012. Climate controls on longshore sediment transport. *Continental Shelf Research,* 48**,** 146-156.

STUMPF, R. P., HOLDERIED, K. & SINCLAIR, M. 2003. Determination of water depth with high-resolution satellite imagery over variable bottom types. *Limnology and Oceanography,* 48**,** 547-556.

SU, H. B., LIU, H. X., WANG, L., FILIPPI, A. M., HEYMAN, W. D. & BECK, R. A. 2014. Geographically Adaptive Inversion Model for Improving Bathymetric Retrieval From Satellite Multispectral Imagery. *Ieee Transactions on Geoscience and Remote Sensing,* 52**,** 465-476.

THOM, B. 1983. Transgressive and regressive stratigraphies of coastal sand barriers in SE Australia. *Marine Geology*.

USGS. 2014. *Landsat Processing Details* [Online]. Available: http://landsat.usgs.gov/Landsat_Processing_Details.php [Accessed 13/09/14 2014].

VAN HETEREN, S., OOST, A. P., VAN DER SPEK, A. J. F. & ELIAS, E. P. L. 2006. Island-terminus evolution related to changing ebb-tidal-delta configuration: Texel, The Netherlands. *Marine Geology,* 235**,** 19-33.

VINTHER, N., NIELSEN, J. & AAGAARD, T. 2004. Cyclic Sand Bar Migration on a Spit-platform in the Danish Wadden Sea—Spit-platform Morphology Related to Variations in Water Level. *Journal of Coastal Research***,** 672-679.

WOODROFFE, C. D. & MURRAY-WALLACE, C. V. 2012. Sea-level rise and coastal change: The past as a guide to the future. *Quaternary Science Reviews,* 54**,** 4-11.

WRIGHT, L. & THOM, B. 1977. Coastal depositional landforms: a morphodynamic approach. *Progress in Physical Geography,* 1.

9 Supplementary material

9.1 Appendix 1: Landsat Data

United States Geological Survey websites to access Landsat image archive

USGS Global Visualisation Viewer:	http://glovis.usgs.gov
USGS Earth Explorer:	http://earthexplorer.usgs.gov
Landsat Look Viewer:	http://landsatlook.usgs.gov

Landsat files used in study

Landsat file	Date of Acquisition	Time of Acquisition (GMT)
LT50890781987142ASA00	22/05/1987	23:05:44.4790560Z
LT50890781988241ASA00	28/08/1988	23:12:31.1070560Z
LT50890781989195ASA00	14/07/1989	23:09:06.0720560Z
LT50890781990182ASA00	1/07/1990	23:01:52.6210690Z
LT50890781991201ASA00	20/07/1991	23:05:07.5980810Z
LT50890781992172ASA00	20/06/1992	23:05:00.5950250Z
LT50890781993142ASA00	22/05/1993	23:04:14.2070690Z
LT50890781994193ASA00	12/07/1994	22:59:55.8370750Z
LT50890781995196ASA02	15/07/1995	22:46:31.1640000Z
LT50890781996231ASA00	18/08/1996	22:57:56.0850940Z
LT50890781997281ASA00	8/10/1997	23:14:47.9380500Z
LT50890781998188ASA00	7/07/1998	23:19:53.7470940Z
LE70890781999215SGS00	3/08/1999	23:34:37.9260517Z
LE70890782000234EDC00	21/08/2000	23:32:44.0394137Z
LE70890782001172ASA00	21/06/2001	23:31:10.6624079Z
LE70890782002287EDC00	14/10/2002	23:29:25.3897720Z
LE70890782003146ASA00	26/05/2003	23:30:25.2386711Z
LT50890782004189ASA00	7/07/2004	23:23:50.7330130Z
LT50890782005255ASA01	12/09/2005	23:29:51.5940250Z
LT50890782006210ASA00	29/07/2006	23:34:56.5340560Z
LT50890782007213ASA00	1/08/2007	23:35:13.9020500Z
LT50890782008296ASA00	22/10/2008	23:25:33.1350130Z
LT50890782009234ASA00	22/08/2009	23:31:09.3300560Z

9.2 Appendix 2: Hydrographic charts data

	1868	1871	1889	1907/43	1955	1967	1985	2009
		From 1868 survey	1869-1870 survey					
Queensland State Archives id								
Title	Wide Bay Bar	Southern Entrance to Great Sandy Strait	East coast of Australia Queensland Moreton Bay to Sandy Cape	Southern portion of Great Sandy strait with Wide bay and harbour	Moreton Bay to Harvey Bay	Moreton Bay to Sandy Cape	Great Sandy Strait Mapping Hydrographic survey	Great Sandy Strait - South
Depth information	Fathoms reduced to low water	Fathoms	Fathoms	Fathoms Reduced 1 foot below mean low water springs	Fathoms reduced to approximately ILWS	Fathoms	Metres Reduced to LWD Using Waddy Point	Metres reduced to LAT
	NB part of channel identical so all charts assumed have levels reduced to 1 foot below MLWS							
	Greatest rise six feet				Datum points Inskip point and Sandy Cape	Datum points Inskip point and Sandy Cape		
Corrections			Major 1889 Minor 1937	Major 1907 Minor 1928 Nb 1945 version Major 1943, but not in study area, both charts identical in study regions		Minor 1972		
Datum standardisation considerations	As these charts have identical soundings in channel, assumption is made that all were reduced to 1 foot below MLWS. Therefore if mean low water is 0.5 metres (at Waddy Point), and 0.5 metres = 1 foot 8 inches then the reduction brings these sounds almost to a reduction to LAT.				ISLW =approx. LAT	Similar sounding values to '55 chart assumption that also LAT	LWD at Waddy Point =LAT for Waddy Point	LAT
All soundings treated as sharing common datum- ie LAT at Waddy Point taken from Queensland Tide Tables Standard Port Tide Times (2014)								

9.3 Appendix 3: ERSI modelbuilder workflows

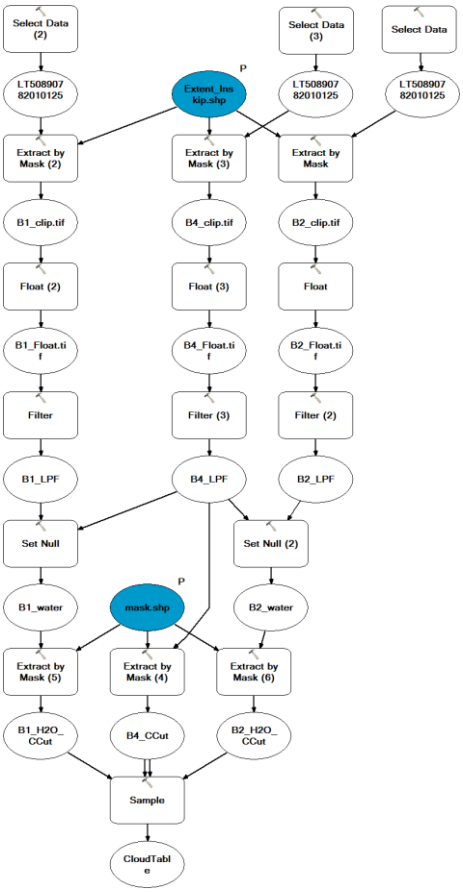

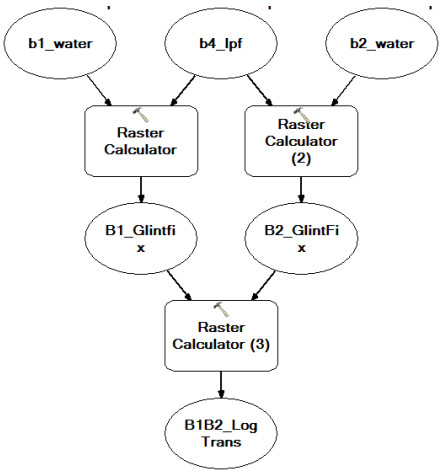

9.4 Appendix 4: LAT adjustment

Landsat file	Date of acquisition	Time of acquisition	Mooloolaba measured tide 23:00 GMT	Mooloolaba measured tide 00:00 GMT	Image capture tide Level	Ebb tode delta water level (Mooloolaba +0.017m)	Ebb tide delta water level rounding to 0.5m	lat 10m @ observation	Number of 0.5m classes	Reduction of depth classes to LAT – reference at 10m terminal lobe contour					
LT50890781987142ASA00	22/05/1987	23:05:44.	0.933*		0.933	0.9	1	11	22	1					
LT50890781988241ASA00	28/08/1988	23:12:31.	1.503		1.503	1.5	1.5	11.5	23	2		1			
LT50890781989195ASA00	14/07/1989	23:09:06.	0.573		0.573	0.6	0.5	10.5	21	3		2		1	
LT50890781990182ASA00	1/07/1990	23:01:52. Z	0.473		0.473	0.5	0.5	10.5	21	4	1	3	1	2	1
LT50890781991201ASA00	20/07/1991	23:05:07.	0.533		0.533	0.6	0.5	10.5	21	5	2	4	2	3	2
LT50890781992172ASA00	20/06/1992	23:05:00.	1.07		1.07	1.1	1	11	22	6	3	5	3	4	3
LT50890781993142ASA00	22/05/1993	23:04:14.	1.29		1.29	1.3	1.5	11.5	23	7	4	6	4	5	4
LT50890781994193ASA00	12/07/1994	22:59:55.	1.33		1.33	1.3	1.5	11.5	23	8	5	7	5	6	5
LT50890781995196ASA02	15/07/1995	22:46:31.	1.37		1.37	1.4	1.5	11.5	23	9	6	8	6	7	6
LT50890781996231ASA00	18/08/1996	22:57:56.	1.45		1.45	1.5	1.5	11.5	23	10	7	9	7	8	7
LT50890781997281ASA00	8/10/1997	23:14:47.	0.82		0.82	0.8	1	11	22	11	8	10	8	9	8
LT50890781998188ASA00	7/07/1998	23:19:53.	0.84		0.84	0.9	1	11	22	12	9	11	9	10	9
LE70890781999215SGS00	3/08/1999	23:34:37.	0.8	1.07	0.935	1.0	1	11	22	13	10	12	10	11	10
LE70890782000234EDC00	21/08/2000	23:32:44.	0.91	1.19	1.05	1.1	1	11	22	14	11	13	11	12	11
LE70890782001172ASA00	21/06/2001	23:31:10.	1.225	0.97	1.0975	1.1	1	11	22	15	12	14	12	13	12
LE70890782002287EDC00	14/10/2002	23:29:25.	0.506	0.598	0.552	0.6	0.5	10.5	21	16	13	15	13	14	13
LE70890782003146ASA00	26/05/2003	23:30:25.	0.758	0.568	0.663	0.7	0.5	10.5	21	17	14	16	14	15	14
LT50890782004189ASA00	7/07/2004	23:23:50.	0.785	0.994	0.8895	0.9	1	11	22	18	15	17	15	16	15
LT50890782005255ASA01	12/09/2005	23:29:51.	0.488	0.602	0.545	0.6	0.5	10.5	21	19	16	18	16	17	16
LT50890782006210ASA00	29/07/2006	23:34:56.	0.975	1.08	1.0275	1.0	1	11	22	20	17	19	17	18	17
LT50890782007213ASA00	1/08/2007	23:35:13.	1.36	1.331	1.3455	1.4	1.5	11.5	23	21	18	20	18	19	18
LT50890782008296ASA00	22/10/2008	23:25:33.	0.505	0.627	0.566	0.6	0.5	10.5	21	22	19	21	19	20	19

LT50890782009234ASA00	22/08/2009	23:31:09.	1.532	1.47	1.501	1.5	1.5	11.5	23	23	20	22	20	21	20
			*measurement from 11/05/1987 corrected via tide curves												

9.5 Appendix 5 Derived Depth imagery